FUNCTIONAL INVESTIGATION OF CRISPR-ENGINEERED SYNONYMOUS DNMT3A MUTATIONS IN CLONAL DOMINANCE OF HEMATOPOIESIS

MARLA NIZA COSTA

A dissertation submitted in partial fulfillment of the requirements for the Degree of Masters in Biomedical Research (Specialization Area: Oncobiology) at Faculdade de Ciências Médicas | NOVA Medical School of NOVA University Lisbon

July, 2025

FUNCTIONAL INVESTIGATION OF CRISPR-ENGINEERED SYNONYMOUS DNMT3A MUTATIONS IN CLONAL DOMINANCE OF HEMATOPOIESIS

Marla Niza Costa
Supervisors: Michael Rieger, Professor and Principal Investigator at Goethe Universitatsklinikum
José António Henriques de Conde Belo, Full Professor at Nova Medical School

A dissertation submitted in partial fulfilment of the requirements for the Degree of Masters in Biomedical Research (Specialization Area: Oncobiology)

July, 2025

The road may have been long and unfamiliar, but every step taken in discomfort has brought me closer to discovery, both within the lab and within myself.

Acknowledgments

I would like to express my deepest gratitude to **NOVA Medical School (NMS)** for providing me with the opportunity to pursue this master's degree and for all the support given throughout the development of this thesis.

I am profoundly thankful to **Prof. Dr. Michael Rieger** for welcoming me into his laboratory in Germany, for offering me this unique opportunity to work within his team, and for enabling me to experience such an enriching scientific and personal journey.

My sincere thanks go to **Dr. Marius Kulp**, who supervised me closely during these months. His unconditional guidance, patience, and availability were invaluable, and I will always be grateful for the knowledge and encouragement he provided every step of the way.

I also wish to extend my gratitude to all the members of the lab, **Tessa Schmachtel, Alec Gessner, Daniel Fischer, HuiMing Tew, Joshua Jambor, Tjeerd Sijmonsma, Ramona Famulla, and Anna Wiegand**, for the friendship, the fun moments, and, of course, for always being ready to help with anything I needed in the lab.

A heartfelt thank you to the friends I made during my time in Germany. Your company helped me maintain a healthy work–life balance and encouraged me to explore and enjoy Germany and other countries. Without you, this experience would not have been the same. To my friends in Portugal, thank you for your endless patience in listening to my complaints and for always being by my side, no matter the distance.

Finally, my deepest gratitude goes to my family, who have always supported and believed in me. A very special thank you to my mother, **Carla Niza**, my greatest supporter and inspiration. None of this would have been possible without her. I can only aspire to become even half the woman she is. And last but not least, thank you to my beloved dog, **Rocky**, for keeping me company and being by my side through everything.

Abstract

Synonymous mutations, once presumed to be biologically silent, are increasingly implicated in the regulation of gene expression and disease pathogenesis. In clonal hematopoiesis of indeterminate potential (CHIP), the DNA methyltransferase DNMT3A is one of the most frequently mutated genes, including at synonymous positions. However, the regulatory consequences of such variants remain largely uncharacterized. In this study, we functionally interrogated synonymous DNMT3A mutations using a dual approach: CRISPR/Cas9-mediated genome editing in THP-1 monocytic cells and overexpression-based transcript decay assays. Genome editing workflows were systematically optimized for suspension hematopoietic cells, identifying the FF100 nucleofection program as optimal for balancing transfection efficiency and cell viability. While homology-directed repair (HDR) remained inefficient despite nocodazole-mediated synchronization, a monoallelic clone bearing a patient-derived synonymous mutation was successfully isolated alongside multiple knockout lines. Western blot and enzymatic assays confirmed almost complete protein and functional loss in specific clones, while others retained partially functional or even hypomorphic DNMT3A variants. Notably, these protein-level effects were not always predictable from genomic edits alone, underscoring the need for direct protein validation. Transcriptomic analysis via RT-qPCR demonstrated that synonymous DNMT3A mutations can significantly modulate mRNA abundance and stability, with individual variants accelerating or delaying transcript decay relative to wildtype. A short 2-hour transcriptional arrest time course further resolved acute stability effects that were masked in longer assays. These findings provide direct evidence that synonymous substitutions in DNMT3A exert functional regulatory effects at the post-transcriptional level, challenging the long-standing assumption of their neutrality. By coupling genome engineering with high-resolution RNA stability profiling, this study expands the functional spectrum of DNMT3A mutations relevant to CHIP and highlights the importance of mRNA-centric regulatory mechanisms in hematopoietic disease.

Resumo

As mutações sinónimas, historicamente consideradas neutras do ponto de vista biológico, têm vindo a ser cada vez mais reconhecidas como moduladores da expressão génica e potenciais contribuintes para a patogénese de várias doenças. No contexto da hematopoiese clonal de potencial indeterminado (CHIP), o gene DNMT3A, codificador de uma DNA metiltransferase essencial, é um dos mais frequentemente mutados, incluindo a nível de posições sinónimas. No entanto, as consequências regulatórias destas variantes permanecem, em grande parte, por esclarecer. Neste estudo, foi realizada uma caracterização funcional de mutações sinónimas em DNMT3A, combinando abordagens de edição genómica via CRISPR/Cas9 em células monocíticas humanas THP-1 com ensaios de sobre-expressão para análise da estabilidade do mRNA. O protocolo de nucleofecção foi sistematicamente optimizado para células hematopoiéticas em suspensão, tendo sido identificado o programa FF100 como o mais eficaz, conciliando eficiência de transfeção com viabilidade celular. Apesar da tentativa de aumentar a eficiência da reparação dirigida por homologia (HDR) através de sincronização do ciclo celular com nocodazol, a maioria dos eventos de reparação ocorreu por junção de extremidades não homólogas (NHEJ). Ainda assim, foi possível isolar um clone monoalélico com uma mutação sinónima derivada de doente, bem como múltiplas linhas knockout. A análise por Western blot e ensaios de atividade enzimática confirmaram a perda completa de proteína e função em determinados clones, enquanto outros revelaram formas hipomórficas ou parcialmente funcionais de DNMT3A. Estes efeitos ao nível proteico não foram sempre previsíveis com base apenas nas alterações genómicas, sublinhando a necessidade de validação funcional direta. A caracterização transcricional por RT-qPCR demonstrou que mutações sinónimas em DNMT3A podem modular significativamente a abundância e estabilidade do mRNA, com variantes individuais a promoverem tanto o aumento como a redução da estabilidade transcricional em relação ao alelo selvagem. Uma análise de curta duração (2 horas) após bloqueio transcricional permitiu identificar efeitos agudos de destabilização, que se encontravam parcialmente mascarados em ensaios de maior duração. Estes resultados constituem evidência direta de que substituições sinónimas em DNMT3A têm efeitos funcionais a nível pós-transcricional, desafiando a tradicional presunção de neutralidade destas variantes. Através da integração de engenharia genómica com perfis de estabilidade de mRNA de alta resolução, este trabalho amplia o espectro funcional de mutações relevantes em DNMT3A no contexto da hematopoiese clonal e destaca a importância de mecanismos regulatórios centrados no mRNA em doenças hematológicas.

Table of Contents

List of Tables

List of Figures

List of Acronyms

CH, Clonal Hematopoiesis

CHIP, Clonal Hematopoiesis of indeterminate potential

DNMT3A, DNA methyltransferase 3a

AML, Acute myeloid leukemia

CVD, Cardiovascular disease

HDR, Homology Directed Repair

HSCs, Hematopoietic Stem Cells

CRISPR-Cas9, Clustered Regularly Interspaced Short Palindromic Repeats and CRISPR-Associated Protein 9

THP-1, Human Leukemia Monocytic Cell Line

TET, ten-eleven translocation family

VAF, Variant Allele Frequency

HSPCs, Hematopoietic stem and progenitor cells

WES, Simple Western™

IL-1β/IL-6, Interleukin-1 beta / Interleukin-6

NLRP3, NOD-like receptor family, pyrin domain containing 3 inflammasome

ASXL1, Additional Sex Combs Like 1

CHD, Coronary Heart Disease

CLP, Common Lymphoid Progenitor

CMP, Common Myeloid Progenitor

DC, Dentritic Cell

DSB, Double-Strand Break

gRNA, Guide RNA

GMP, Granulocyte-Macrophage Progenitor

HSPC, Hematopoietic Stem and Progenitor Cell

JAK2, Janus Kinase 2

LT-HSC, Long-Term Hematopoietic Stem Cell

MEP, Megakaryocyte-Erythrocyte Progenitor

MPP, Multipotent Progenitor

NHEJ, Non-Homologous End Joining

NK, Natural Killer Cell

PAM, Protospacer Adjacent Motif

RNP, Ribonucleoprotein

ROS, Reactive Oxygen Species

sgRNA, Single-Guide RNA

SRSF2, Serine and Arginine Rich Splicing Factor 2

ST-HSC, Short-Term Hematopoietic Stem Cell

TP53, Tumor Protein p53

U2AF1, U2 Small Nuclear RNA Auxiliary Factor 1

1. Introduction

1.1. Hematopoiesis and Clonal Dominance

Hematopoiesis is the tightly regulated biological process by which the body generates all mature blood cell types from a pool of undifferentiated hematopoietic stem cells (HSCs). This process occurs predominantly in the bone marrow and ensures continuous production of erythrocytes, leukocytes, including neutrophils, eosinophils, basophils, monocytes/macrophages, T lymphocytes, B lymphocytes, and natural killer (NK) cells, as well as thrombocytes (platelets) derived from megakaryocytes (Belyavsky et al., 2021; Udroiu & Sgura, 2021). On average, approximately 100 billion blood cells are produced per day in healthy adult humans to maintain hematopoietic homeostasis and support immune surveillance, oxygen transport, and hemostasis. At the apex of the hematopoietic hierarchy are long-term repopulating hematopoietic stem cells (LT-HSCs), a rare population of quiescent, self-renewing cells characterized by multipotency, the capacity to generate all mature hematopoietic lineages (Komic et al., 2025). These HSCs give rise to short-term HSCs and a broader pool of hematopoietic progenitor cells (HPCs), including multipotent progenitors (MPPs), which lack long-term self-renewal capacity but retain lineage plasticity. Further lineage commitment results in the formation of oligopotent progenitors such as common myeloid progenitors (CMPs) and common lymphoid progenitors (CLPs), which then differentiate into mature cell types through defined transcriptional and epigenetic programs (Laurenti & Göttgens, 2018; Mende & Laurenti, 2021). HSC fate is governed by a dynamic balance between quiescence, symmetric self-renewal (producing two daughter HSCs), asymmetric division (producing one HSC and one progenitor cell), and differentiation. Under homeostatic conditions, the majority of LT-HSCs are maintained in a quiescent (G_0) state within specialized bone marrow niches. These niches supply essential nutrients and “state-maintaining” cytokines and likely shield LT-HSCs from immune-mediated attacks. The protection from replication-induced DNA damage, however, arises specifically from their quiescent state itself, as cells in G_0 do not enter S-phase and therefore avoid DNA replication–associated lesions, thereby preserving their long-term regenerative potential (Eaves, 2015). However, in response to physiological stressors such as infection, hemorrhage, or inflammation, HSCs are rapidly activated to proliferate and replenish blood cell populations (Zhao & Deininger, 2023; Komic et al., 2025).

The prolonged lifespan and replicative capacity of HSCs predispose them to the gradual accumulation of somatic mutations. While many of these mutations are functionally neutral, some confer a competitive advantage, enabling specific clones to expand disproportionately within the hematopoietic compartment. This phenomenon, known as clonal hematopoiesis (CH), is defined by the expansion of hematopoietic clones

harboring recurrent somatic mutations in the absence of cytopenias or hematologic malignancy (Yamashita et al., 2020; Kusne et al., 2022; Ortmann et al., 2019).

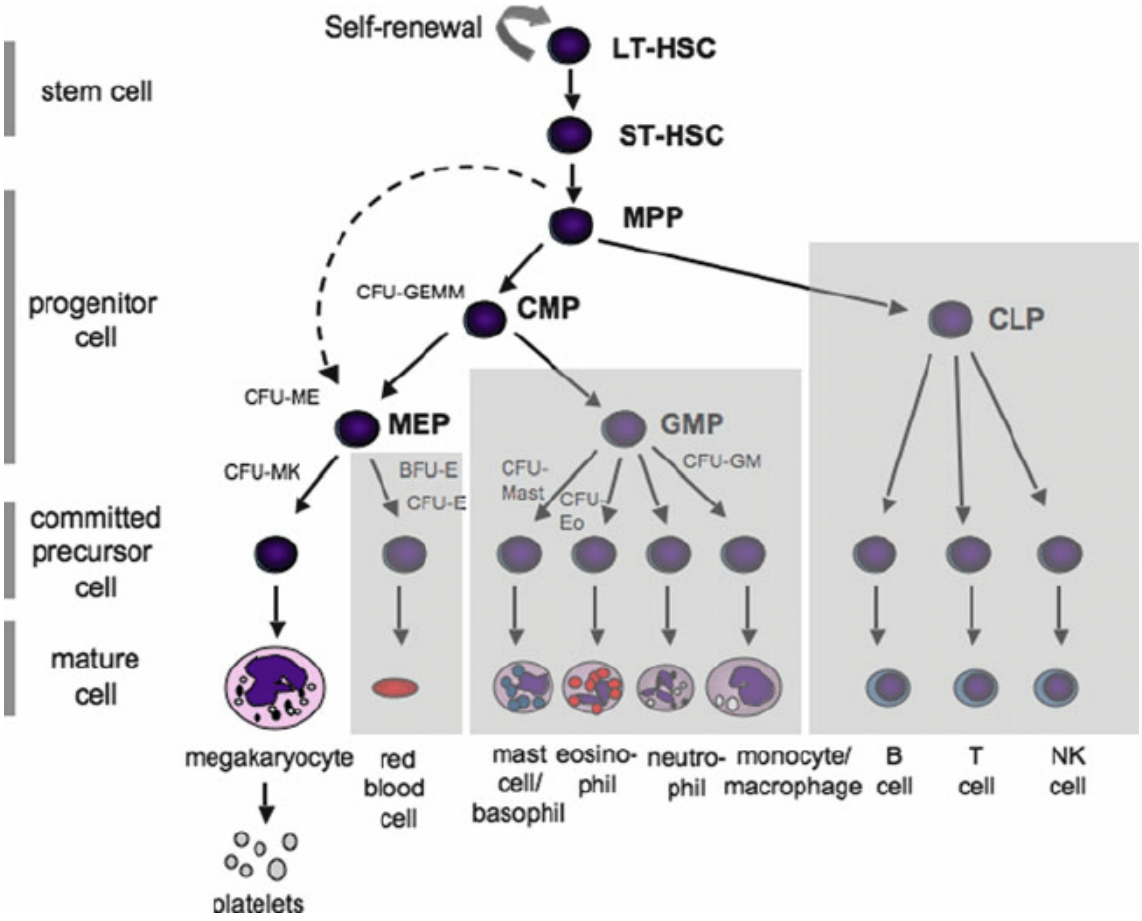

Figure 1. Taken from Yamashita et al., 2020. The human hematopoietic hierarchy. LT-HSC = Long-term hematopoietic stem cell. ST-HSC = Short-term hematopoietic stem cell. MPP = Multipotent progenitor. CLP = Common lymphoid progenitor. CMP = Common myeloid progenitor. MEP = Megakaryocyte–erythrocyte progenitor. GMP = Granulocyte–macrophage progenitor. B = B cell. T = T cell. NK = Natural killer cell. DC = Dendritic cell. E = Erythrocyte. Mk = Megakaryocyte. G = Granulocyte. Mac = Macrophage.

CH is thought to originate from single HSCs or early progenitor cells that acquire mutations affecting genes involved in epigenetic regulation (*DNMT3A*, *TET2*, *ASXL1*), RNA splicing (*SRSF2*, *SF3B1*, *U2AF1*), signal transduction (*JAK2*, *CBL*), or DNA damage response (*TP53*) (Noubouossie et al., 2017). These mutations confer increased self-renewal, resistance to apoptosis, or enhanced inflammatory resilience, promoting clonal outgrowth and displacement of wild-type HSCs (Greaves & Maley, 2012; von Bonin et al., 2021). Clonal hematopoiesis is detectable through high-depth next-generation sequencing of peripheral blood mononuclear cells, with prevalence increasing sharply with age, approximately 10% of individuals aged 65 and over, and over 20% of those aged 80 and above, carry detectable CH-associated mutations (Fuster et al., 2018).

A clinically defined subset of CH, termed clonal hematopoiesis of indeterminate potential (CHIP), is diagnosed when a somatic mutation in a leukemia-associated driver gene is present at a variant allele frequency (VAF) of ≥2% without accompanying cytopenias or evidence of a hematologic neoplasm (Marnell et al., 2021; Reed et al., 2023). CHIP is associated with a 0.5–1.0% annual risk of progression to hematologic malignancies, particularly myelodysplastic syndromes (MDS) and acute myeloid leukemia (AML) (Genovese et al., 2014). However, recent studies have also shown that CH, even in the absence of CHIP-level mutations, is associated with elevated risks of cardiovascular disease, atherosclerosis, ischemic stroke, and overall mortality (Jaiswal & Ebert, 2019; Xie & Zeidan, 2023). The pathobiology of CHIP and CH involves the expansion of HSC clones with altered transcriptional, inflammatory, and metabolic profiles. For example, loss-of-function mutations in *TET2* and *DNMT3A* have been shown to reduce DNA demethylation and alter cytokine signaling pathways, enabling clonal dominance in pro-inflammatory microenvironments (Wang et al., 2022). Such mutated clones produce myeloid-biased progeny with increased secretion of inflammatory mediators (e.g., IL-6, TNF-α), which can exacerbate vascular dysfunction and contribute to non-hematologic pathology (Cai et al., 2018; Tall & Fuster, 2022). These findings reinforce that CH is not merely a precursor to leukemia but a systemic condition with broad clinical relevance (Caiado et al., 2025).

The development of CH is driven by both intrinsic (genetic/epigenetic) and extrinsic (environmental) factors. Aging remains the strongest known risk factor, but exposure to ionizing radiation, cytotoxic chemotherapy, tobacco smoke, and chronic inflammation significantly accelerates the acquisition and selection of pathogenic mutations (Fujino et al., 2022). Notably, even in the absence of progression to malignancy, the presence of CH or CHIP is associated with adverse outcomes and warrants consideration in both clinical and research settings (Reed et al., 2023).

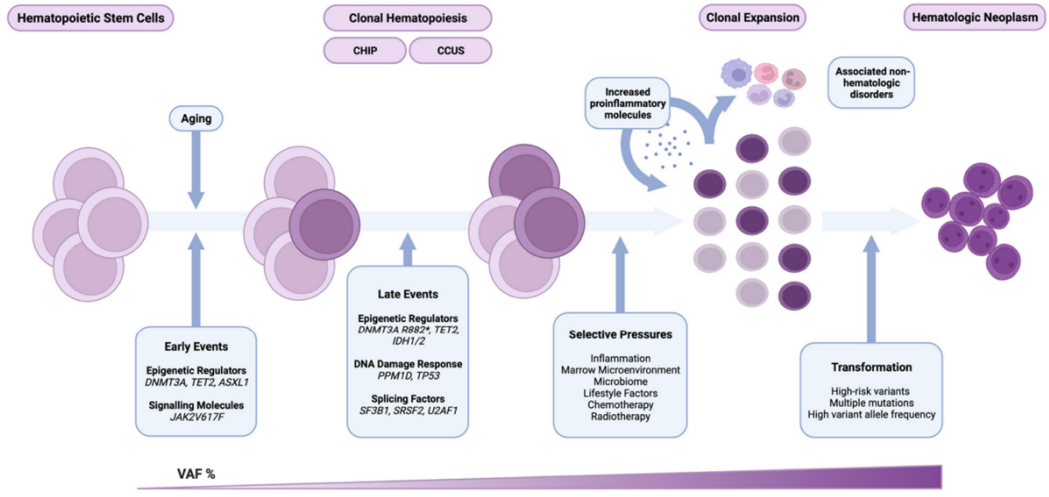

Figure 2. Taken from Gaulin et al., 2022. Molecular pathways in clonal hematopoiesis of indeterminate potential (CHIP). HSC = Hematopoietic stem cell. CHIP = Clonal hematopoiesis of indeterminate potential. DNMT3A = DNA methyltransferase 3A. TET2 = Tet methylcytosine dioxygenase 2. ASXL1 = Additional sex combs-like 1. PPM1D = Protein phosphatase, Mg2+/Mn2+ dependent 1D. TP53 = Tumor protein p53. JAK2 = Janus kinase 2. ROS = Reactive oxygen species. CVD = Cardiovascular disease. AML = Acute myeloid leukemia.

1.2. The Impact of Clonal Hematopoiesis on Chronic Heart Diseases

Beyond its role in hematologic contexts, CHIP has been identified as a significant age-related risk factor for non-hematologic conditions, most notably cardiovascular disease (CVD) (Zha et al., 2024). Population-based genomic studies indicate that by age 70, between 20% and 50% of individuals harbor a detectable CHIP clone, defined by somatic mutations in leukemia-associated genes at variant allele frequencies (VAFs) ≥2% (Natarajan et al., 2023). Importantly, CHIP is associated with a ~1.9-fold increased risk of incident coronary heart disease (CHD) and stroke (Todorovski et al., 2025), and an estimated 40% increase in all-cause mortality, primarily attributable to cardiovascular morbidity (Cao et al., 2023). CHIP carriers experiencing myocardial infarction, heart failure, or cardiogenic shock have consistently poorer outcomes, including higher mortality and increased incidence of recurrent events (Doehner et al., 2023; Dorsheimer et al., 2020).

Mechanistically, CHIP drives cardiovascular pathology through dysregulated immune responses and chronic low-grade inflammation (Wang et al., 2025). Mutations in CHIP-associated genes, particularly *DNMT3A* and *TET2*, skew myeloid cell differentiation, enhance IL-1β and IL-6 production, and potentiate NLRP3 inflammasome activation, contributing to accelerated atherogenesis and impaired cardiac remodeling (Gonzalez et al., 2024). These mutant myeloid cells exhibit prolonged lifespan, altered metabolic profiles, and increased tissue infiltration, establishing a feedforward loop in which inflammation promotes further clonal expansion (Strauss et al., 2021).

Among CHIP-associated mutations, those in *DNMT3A* (DNA methyltransferase 3 alpha) are by far the most prevalent, accounting for 35–45% of all CHIP cases (Venugopal et al., 2021; Marnell et al., 2021). Initially identified in acute myeloid leukemia (AML) as early founder lesions (Ley et al., 2010; Yan et al., 2011), *DNMT3A* mutations are predominantly missense substitutions at residue R882 (disrupting tetramer formation) or loss-of-function truncating variants. These mutations impair *DNMT3A*'s function as a *de novo* methyltransferase responsible for catalyzing cytosine methylation at CpG dinucleotides, genomic regions where a cytosine is followed by a guanine in the 5' to 3' direction, and which serve as regulatory hotspots enriched in gene promoters, enhancers, and transcription factor binding sites (Challen et al., 2012). Proper methylation of CpG elements is essential for epigenetic silencing of lineage-inappropriate genes and maintenance of hematopoietic stem cell identity (Krämer, 2023). Disruption of *DNMT3A*-mediated CpG methylation leads to focal hypomethylation, particularly at distal enhancers and polycomb-regulated loci, resulting in aberrant expression of genes involved in stem cell maintenance and immune signaling (Guo, 2023). Functionally, *Dnmt3a*-deficient murine HSCs demonstrate a significantly increased self-renewal capacity, reduced myeloid and lymphoid differentiation, and outcompete wild-type HSCs in serial transplantation assays (Gundry et al., 2016). These clones exhibit enhanced proliferation, resistance to

apoptosis, and impaired repression of proinflammatory programs via IL-6/STAT3 signaling, contributing to both clonal dominance and systemic inflammation (Bhat et al., 2022). From a cellular perspective, *DNMT3A*-mutant clones display impaired DNA damage responses, increased proliferation, and enhanced cytokine signaling via the IL-6/STAT3 axis (Kallikourdis et al., 2025). Somatic mosaicism in *DNMT3A*, when confined to hematopoietic lineages, exemplifies the principles of selective somatic evolution (Nam et al., 2022). Most mutations that arise in somatic tissues due to endogenous replication errors or environmental insults are either neutral, having no measurable effect on cellular function, or deleterious, impairing gene expression, protein function, or regulatory integrity. While some neutral mutations are synonymous (silent) mutations that do not change the amino acid sequence, functional neutrality can also arise from non-synonymous or non-coding mutations that do not affect cellular fitness (Vijg et al., 2023). Neutral mutations typically accumulate passively in noncoding or non-functional regions and do not alter cell behavior (Díaz Navarro, 2022). In contrast, deleterious mutations disrupt essential cellular processes, such as DNA replication, cell cycle regulation, or metabolic homeostasis, and are subject to purifying selection, leading to their removal via intrinsic apoptosis, stress-induced senescence, or immune-mediated clearance (Yang et al., 2025). These mutations, which frequently affect the methyltransferase domain (e.g., R882H/C) or truncate the protein, result in partial loss-of-function phenotypes that reprogram the DNA methylation landscape without inducing cytotoxic stress (Karpova et al., 2025). Consequently, *DNMT3A*-mutant hematopoietic stem cells (HSCs) retain viability while acquiring a selective advantage characterized by enhanced self-renewal, impaired differentiation, and increased resistance to apoptotic cues (Huang et al., 2024). Empirical estimates from longitudinal sequencing data indicate that these mutant clones expand at a rate of approximately 10–15% per year, particularly within aged HSC compartments or under genotoxic stress, such as cytotoxic therapy or chronic inflammation (Buscarlet et al., 2017). The persistence and expansion of such clones emphasizes the capacity of specific somatic mutations to circumvent negative selection and reshape hematopoietic architecture through non-malignant, yet pathophysiological significant, clonal dominance (Mitra et al., 2024).

Taken together, *DNMT3A* mutations represent a prototypical driver of age-related clonal hematopoiesis (Fabre et al., 2025). Their high prevalence defines epigenetic mechanisms, and the pleiotropic impact on immune function and inflammation provides a compelling rationale for focused investigation. CHIP, and *DNMT3A*-driven clones in particular, represent a bridge between somatic evolution, epigenetic deregulation, and non-malignant disease progression.

1.3. DNTM3A Synonymous Mutations: Silent Changes with Functional Consequences

The human *DNMT3A* gene spans 23 exons on chromosome 2p23.3 and gives rise to multiple isoforms through alternative splicing, with two predominant protein products: DNMT3A1 (130 kDa) and DNMT3A2 (100 kDa) (Huang & Aghaei-Zarch, 2024; Venugopal et al., 2021). DNMT3A1 includes a complete N-terminal regulatory

domain, while DNMT3A2 lacks the first 219 amino acids, which alters its nuclear localization and chromatin targeting (Smith & Meissner, 2013). In the hematopoietic system, *DNMT3A* is robustly expressed in LT-HSCs and ST-HSCs, MPPs, and committed myeloid progenitors, with expression decreasing progressively during terminal differentiation (Chen et al., 2023).

Pathogenic *DNMT3A* variants observed in CHIP and hematologic malignancies comprise a broad spectrum of alterations, including missense mutations, most commonly at the R882 codon within the C-terminal catalytic domain, which destabilize the tetrameric conformation required for full enzymatic activity; nonsense mutations that introduce premature stop codons and result in truncated, non-functional proteins; frameshift insertions or deletions that trigger nonsense-mediated decay. In addition, splice-site mutations frequently compromise the integrity of specific exons. Importantly, these exons may be coding exons, which directly contribute nucleotide sequences that are translated into the protein, or regulatory/non-coding exons, which are transcribed but not translated and instead play essential roles in regulating splicing, transcript stability, or translation efficiency. Disruption of either class can lead to aberrant DNMT3A isoforms with impaired or altered function, underscoring the critical contribution of both coding and non-coding elements to the gene's proper expression and enzymatic activity (Grossmann et al., 2011). The R882H and R882C mutations, in particular, confer dominant-negative effects by incorporating catalytically inactive subunits into functional methyltransferase complexes, thereby suppressing DNA methylation even in the presence of a wild-type allele (Kunert, 2024). Both monoallelic and biallelic mutations have been reported, with monoallelic variants being significantly more prevalent in CHIP and adult acute myeloid leukemia (AML), whereas biallelic lesions are rare and often associated with aggressive disease phenotypes (Klco et al., 2021).

Functionally, *DNMT3A* mutations, especially loss-of-function frameshift and R882 substitutions, induce global and site-specific hypomethylation at CpG dinucleotides, particularly in intergenic enhancers, polycomb-regulated regions, and developmentally important promoters (Li, 2023). CpG dinucleotides are cytosine-guanine nucleotides connected by a phosphodiester bond on the same DNA strand. These sites serve as key genomic elements where DNA methylation typically represses transcriptional activation (Zahoor et al., 2025). Proper methylation of CpG sites ensures the stable repression of lineage-inappropriate or stemness-related genes, a process required for epigenetic homeostasis and fidelity of lineage commitment. Disruption of this repression in *DNMT3A*-mutant cells leads to derepression of self-renewal-associated genes, such as *Meis1*, *Gata2*, and *Hox* family members, while concurrently impeding the activation of differentiation-specific programs (Ferreira et al., 2016; Jeong et al., 2018). This shift in the epigenetic landscape results in hematopoietic stem cell expansion, delayed differentiation, and the persistence of clonally derived multipotent progenitors (Brown, 2022). Mouse models of conditional *Dnmt3a* deletion exhibit enhanced serial repopulation potential, resistance to apoptosis, and accumulation of transcriptionally

dysregulated HSCs (Hormaechea-Agulla et al., 2021). However, these models typically do not develop leukemia in the absence of additional cooperating mutations, indicating that *DNMT3A* mutations prime the hematopoietic compartment for transformation but are insufficient to drive leukemogenesis independently (Basheer et al., 2021).

The role of *DNMT3A* must be contextualized within the broader dynamics of DNA methylation, which is regulated by three primary methyltransferases: DNMT1, DNMT3A, and DNMT3B (Tajima et al., 2022). DNMT1 maintains existing methylation patterns during S-phase by recognizing hemi-methylated DNA and restoring full methylation on daughter strands. Loss of DNMT1 activity during replication leads to passive demethylation, resulting in transcriptional instability and impaired cell fate fidelity (Turpin et al., 2022). In contrast, DNMT3A and DNMT3B catalyze *de novo* methylation during development and in response to lineage-instructive cues (Smith & Meissner, 2013). The methylation marks they establish are reversible through the action of the ten-eleven translocation (TET) dioxygenase family (TET1, TET2, TET3), which oxidize 5-methylcytosine (5mC) to 5-hydroxymethylcytosine (5hmC) and promote active demethylation. Loss-of-function mutations in TET2, another gene commonly mutated in CHIP, result in aberrant DNA hypermethylation (Ito et al., 2010, 2011; Ko et al., 2010). In contrast, *DNMT3A* mutations, particularly those involving catalytic domain disruption, lead to persistent hypomethylation of critical hematopoietic regulatory loci. These methylation defects are not only present in leukemic cells but also in phenotypically normal clonal HSCs, establishing an epigenetic substrate for malignant progression (Buscarlet et al., 2017).

Although regarded as biologically inert, synonymous mutations in *DNMT3A* are increasingly implicated in functional dysregulation (Lue, 2023). Synonymous mutations are nucleotide substitutions occurring within coding sequences that do not result in an amino acid change due to the redundancy of the genetic code (Sauna & Kimchi-Sarfaty, 2011). Recent studies demonstrate that synonymous substitutions can alter mRNA secondary structure, codon usage bias, translational kinetics, and even exon inclusion by modulating splicing enhancer or silencer elements (Oelschlaeger, 2024). In *DNMT3A*, synonymous variants may therefore affect isoform ratios, ribosomal pausing, or post-transcriptional regulation, contributing subtly but significantly to altered protein abundance or folding dynamics (Zhang, 2023). These effects may be particularly relevant in the context of CHIP, where even small perturbations in enzyme activity can shift the clonal fitness landscape.

The clinical implications of *DNMT3A* mutations extend beyond hematologic malignancy (Khrabrova, 2021; Jaiswal et al., 2017). CHIP driven by *DNMT3A* mutations is increasingly recognized as a major independent risk factor for cardiovascular disease, particularly heart failure and post-infarction complications (Jaiswal et al., 2017; Sano et al., 2018; Yu et al., 2023). Clinical cohort studies have demonstrated that individuals with CHIP carrying *DNMT3A* or *TET2* mutations exhibit increased mortality following myocardial infarction and are at higher risk of developing chronic heart failure (Jaiswal et al., 2017;

Yu et al., 2023). The mechanistic basis involves altered immune cell output from mutant clones, leading to skewing of monocytes and macrophages toward a pro-inflammatory phenotype, enhanced IL-1β production, and activation of the NLRP3 inflammasome (Sano et al., 2018; Fuster et al., 2017). These inflammatory pathways contribute to endothelial dysfunction, cardiac fibrosis, and adverse remodeling (Fuster et al., 2017; Sano et al., 2018). Experimental murine models of Dnmt3a-deficient hematopoiesis confirm that inhibition of IL-1β signaling can ameliorate left ventricular dysfunction, highlighting the therapeutic relevance of targeting inflammatory circuits in CHIP-related cardiovascular disease (Sano et al., 2018). Moreover, mosaic loss of the Y chromosome (LOY), which frequently co-occurs with DNMT3A mutations in aging males, further amplifies cardiac risk by impairing immune surveillance and promoting profibrotic myeloid activation (Sano et al., 2022). Collectively, these findings emphasize the pathogenic relevance of *DNMT3A* mutations in systemic disease and establish CHIP as a critical determinant of cardiovascular outcomes (Yu et al., 2023; Sano et al., 2022).

1.4. Molecular Mechanisms of DNMT3A in Epigenetic Regulation

Epigenetic regulation is particularly relevant in the context of DNMT3A, where precise spatiotemporal control of transcript and protein abundance is essential for the maintenance of hematopoietic stem cell identity and epigenetic homeostasis (Guryanova et al., 2016; Gaulin et al., 2022).

Mechanistically, synonymous mutations may alter the thermodynamic stability and secondary structure of mRNA, thereby influencing transcript folding, subcellular localization, and interactions with RNA-binding proteins (Hunt et al., 2014; Shen et al., 2022). Altered mRNA conformation can perturb the efficiency of ribosome loading and elongation, with consequences for translation fidelity and the kinetics of co-translational protein folding (Sauna & Kimchi-Sarfaty, 2011; Supek et al., 2014). Codon usage bias, shaped by the differential abundance of tRNA isoacceptors, determines translation elongation rates and is tightly coupled to nascent chain folding trajectories (Hanson & Coller, 2018). Substitution of a frequently used (optimal) codon with a rare synonymous codon can induce ribosomal pausing or stalling, increasing the risk of translational infidelity or proteostatic stress (Sauna & Kimchi-Sarfaty, 2011; Shen et al., 2022). Conversely, replacement of a suboptimal codon with a more efficiently decoded synonym may accelerate elongation and disrupt the folding of discrete protein domains. These effects are particularly consequential for multidomain proteins or enzymes with stringent structural requirements, such as DNMT3A (Guryanova et al., 2016).

In addition to modulating translation dynamics, synonymous mutations can interfere with the fidelity of pre-mRNA splicing. Although they do not alter the encoded amino acid, these substitutions can disrupt exonic splicing enhancers or silencers, which are critical for accurate recognition of exon-intron junctions by the spliceosome (Supek et al., 2014; Hunt et al., 2014). Functional disruption of these cis-regulatory elements

can result in aberrant exon skipping, intron retention, or activation of cryptic splice sites. In genes with complex splicing architectures or weak consensus splice motifs, such as DNMT3A, these alterations may generate aberrant isoforms with modified stability, localization, or enzymatic function (Gaulin et al., 2022; Guryanova et al., 2016). Moreover, changes to exon definition may affect the inclusion of regulatory protein domains, thereby compromising catalytic activity or interaction with chromatin-associated partners (Guryanova et al., 2016).

Synonymous mutations may also affect mRNA half-life by altering codon usage or disrupting regulatory motifs embedded within the coding region. Codon identity and distribution can influence the recruitment of RNA-binding proteins that modulate transcript decay through deadenylation, decapping, or nonsense-mediated decay pathways (Hanson & Coller, 2018; Hunt et al., 2014). Consequently, synonymous variants can shift the steady-state abundance of the mRNA transcript independently of transcriptional regulation, leading to quantitative alterations in protein output. This phenomenon is particularly relevant in genes such as DNMT3A, where tight regulation of protein expression is essential, and even minor deviations in protein levels can disrupt epigenetic programming and compromise lineage fidelity in hematopoietic stem cells (Gaulin et al., 2022; Guryanova et al., 2016).

In clonal hematopoiesis, where selection acts gradually on small differences in cellular fitness, subtle changes in DNMT3A expression or activity resulting from synonymous mutations may yield a measurable selective advantage at the clonal level (Gaulin et al., 2022; Shen et al., 2022). While the majority of CHIP-associated DNMT3A mutations are protein-altering (e.g., R882H/C or frameshifts), the potential contribution of synonymous mutations to clonal selection has been underexplored. Recent studies integrating codon substitution models, RNA secondary structure predictions, and ribosome profiling suggest that select synonymous variants in regulatory genes may be subject to positive selection, particularly when affecting translational efficiency, splicing fidelity, or transcript stability (Shen et al., 2022; Supek et al., 2014).

Taken together, these findings highlight that synonymous mutations, although silent at the level of primary protein sequence, can modulate multiple layers of gene expression regulation. In the case of DNMT3A, such variants may influence the epigenetic landscape indirectly by altering protein dosage, folding dynamics, or isoform composition, thereby contributing to hematopoietic clonal expansion and disease predisposition (Gaulin et al., 2022; Guryanova et al., 2016). Continued investigation into the non-canonical effects of synonymous variation is warranted to elucidate their functional relevance in clonal hematopoiesis and related pathologies (Shen et al., 2022; Supek et al., 2014).

1.5. CRISPR/Cas9 as a Tool for Genome Editing

CRISPR/Cas9 genome editing represents a fundamental advancement in molecular biology, enabling precise and programmable modification of endogenous genomic loci in mammalian cells (Doudna & Charpentier, 2014; Hsu et al., 2014). This system, derived from the adaptive immune machinery of prokaryotes, comprises a single-guide RNA (sgRNA) that directs the Cas9 endonuclease to a complementary DNA sequence adjacent to a protospacer adjacent motif (PAM), typically 5'-NGG-3' for Streptococcus pyogenes Cas9 (SpCas9) (Jinek et al., 2012; Hsu et al., 2014). Upon DNA binding, Cas9 introduces a double-strand break (DSB) three nucleotides upstream of the PAM site (Jinek et al., 2012).

The cellular response to Cas9-mediated DSBs is governed by two principal DNA repair pathways: non-homologous end joining (NHEJ) and homology-directed repair (HDR) (Ceccaldi et al., 2016; Yeh et al., 2019). NHEJ is an error-prone mechanism active throughout the cell cycle and is the predominant repair pathway in most mammalian cell types. It rejoins DNA ends without a homologous template, frequently introducing small insertions or deletions (indels) at the cleavage site, thereby disrupting open reading frames and leading to gene knockout (Ceccaldi et al., 2016; Yeh et al., 2019). HDR, by contrast, is a high-fidelity repair mechanism that utilizes a homologous donor DNA template, either a single-stranded oligodeoxynucleotide (ssODN) or double-stranded DNA (dsDNA), to precisely repair the DSB. This pathway enables the introduction of defined nucleotide substitutions, small insertions, or epitope tags (Yeh et al., 2019; Richardson et al., 2016). HDR is predominantly active during the S and G2 phases of the cell cycle, and strategies to enhance HDR efficiency include cell cycle synchronization, small-molecule inhibition of NHEJ (e.g., DNA-PK inhibitors), and optimized design of homology arms (Maruyama et al., 2015; Yeh et al., 2019).

CRISPR/Cas9 components can be delivered into mammalian cells in various formats: plasmid DNA encoding Cas9 and sgRNA, in vitro transcribed mRNA (allowing for transient Cas9 expression), or preassembled ribonucleoprotein (RNP) complexes composed of recombinant Cas9 protein and synthetic sgRNA (Kim et al., 2014; Liang et al., 2015; Lino et al., 2018). Among these, RNP delivery is advantageous due to its immediate

activity upon cytoplasmic entry and transient expression profile, which minimizes off-target effects and genomic integration risks (Kim et al., 2014; Liang et al., 2015).

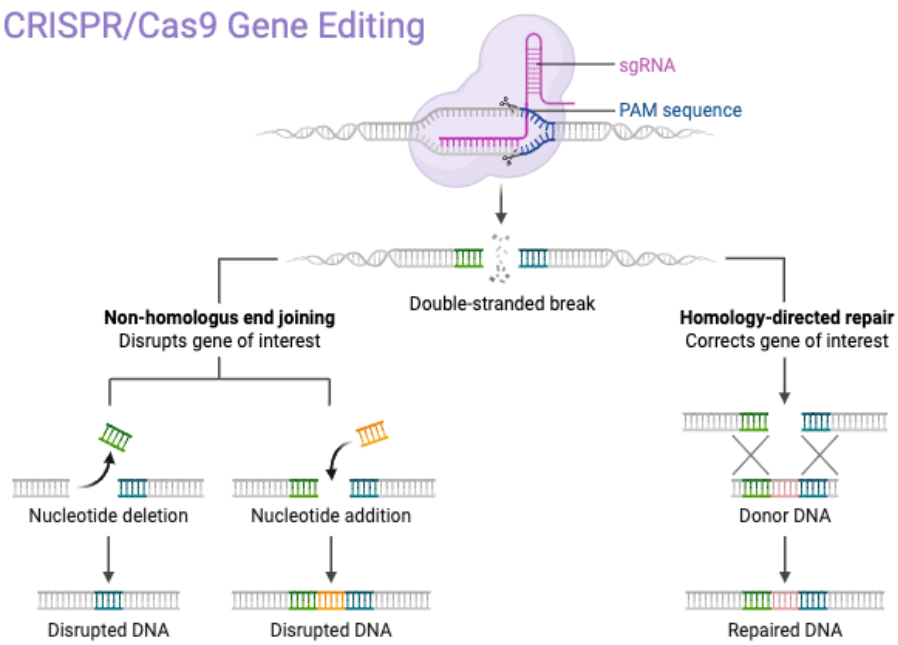

Figure 3. ***CRISPR/Cas9 gene editing outcomes via non-homologous end joining (NHEJ) and homology-directed repair (HDR).*** Cas9, guided by a single-guide RNA (sgRNA), introduces a double-strand break at a specific genomic site near a PAM sequence. The break can be repaired by NHEJ, which often causes insertions or deletions that disrupt the gene, or by HDR, which uses a donor DNA template to introduce precise genetic changes. Figure created with BioRender.com.

Multiple delivery platforms have been developed to facilitate the intracellular uptake of CRISPR/Cas9 components (Lino et al., 2018; Wang et al., 2023). Electroporation and nucleofection are widely used for both adherent and suspension cells, including primary cells, due to their capacity to transiently permeabilize the plasma membrane via electrical pulses, allowing direct entry of RNPs or nucleic acids into the cytoplasm and nucleus (Kim et al., 2014; Lino et al., 2018). Nucleofection, a variant of electroporation optimized for nuclear delivery, has shown superior efficiency in hard-to-transfect cell types, including hematopoietic stem and progenitor cells (Lino et al., 2018; Mock et al., 2014). Lipofection utilizes cationic lipid-based carriers that encapsulate CRISPR components and mediate cellular uptake through endocytosis, while suitable for adherent cell lines, its efficiency is reduced in primary or suspension cells (Lino et al., 2018; Wang et al., 2023). Viral vectors, such as lentiviruses and adeno-associated viruses (AAV), offer high transduction efficiency and sustained expression of CRISPR elements, but raise concerns related to insertional mutagenesis and long-term Cas9 activity, making them less desirable for applications requiring transient expression or clinical translation (Lino et al., 2018; Wang et al., 2023).

To mitigate off-target activity, numerous high-fidelity Cas9 variants (e.g., SpCas9-HF1, eSpCas9, HypaCas9) and truncated sgRNAs have been developed to enhance sequence specificity (Kleinstiver et al., 2016; Slaymaker et al., 2016; Chen et al., 2017). Computational tools integrating chromatin accessibility, GC content, and sequence context are also employed to optimize sgRNA design and minimize unintended genomic alterations (Doench et al., 2016; Wang et al., 2023). Additionally, emerging platforms such as base editors and prime editors offer DSB-independent genome modification by catalyzing single-nucleotide conversions or small edits via tethered deaminase or reverse transcriptase domains, thereby expanding the functional capacity of CRISPR systems while reducing genotoxic risk (Anzalone et al., 2020; Komor et al., 2016; Wang et al., 2023).

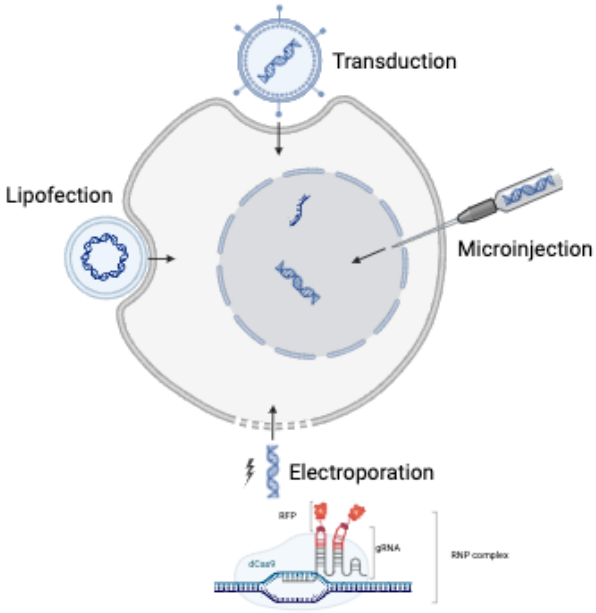

Figure 4. ***Overview of common delivery methods for CRISPR/Cas9 components.*** Gene editing tools such as plasmid DNA, RNA, or ribonucleoprotein complexes (RNPs) can be introduced into cells through various methods: lipofection (lipid-mediated uptake), electroporation (electric field-induced membrane permeabilization), microinjection (direct cytoplasmic or nuclear delivery), and viral transduction (vector-mediated gene transfer using viruses such as lentivirus or AAV). Each method varies in efficiency, cell type compatibility, and risk of genomic integration. Figure created with BioRender.com.

In summary, CRISPR/Cas9 genome editing enables targeted gene disruption via NHEJ and precise sequence modification via HDR, facilitated by a diverse array of delivery strategies tailored to specific cell types and experimental objectives (Doudna & Charpentier, 2014; Lino et al., 2018; Yeh et al., 2019). Continued refinement of editing fidelity, delivery efficiency, and repair pathway modulation will further enhance the utility of CRISPR/Cas9 as a tool for dissecting gene function and modeling human disease (Hsu et al., 2014; Yeh et al., 2019; Wang et al., 2023).

2. Hypothesis and aims

This project investigates the hypothesis that synonymous mutations in the *DNMT3A* gene, mutations traditionally considered silent due to their minimal impact on amino acid sequences, can, in fact, influence gene function and contribute to disease. Although these variants do not alter protein coding, their presence in patients with chronic heart failure and their known involvement in leukemia suggest they may play a regulatory role at the RNA or translational level. This research aims to uncover the molecular mechanisms through which such mutations affect *DNMT3A* function, potentially by altering mRNA stability, splicing, or translation efficiency, thereby challenging the conventional view of synonymous mutations as biologically neutral.

Aims of the research:

1. To employ CRISPR/Cas9 genome editing to introduce patient-derived synonymous DNMT3A mutations into the THP-1 myeloid cell line, enabling precise modeling of these variants in a relevant cellular context.
2. To determine whether synonymous DNMT3A mutations, despite preserving the encoded amino acid sequence, can alter DNMT3A function and thereby contribute to pathogenic mechanisms.
3. To elucidate the molecular consequences of synonymous DNMT3A mutations by systematically assessing their impact on mRNA stability, splicing patterns, transcriptional and translational fidelity, ribosome pausing dynamics, and protein folding.

3. Organisms, materials, and methods

3.1. Organisms

3.1.1. Human Cell Line

The cell line used for implementing the DNMT3A mutations was THP-1**,** a human monocytic leukemia cell line obtained from DSMZ (German Collection of Microorganisms and Cell Cultures, ACC 16)**.**

Stable cell culture models were established using THP-1 cells, which were maintained in RPMI 1640 medium supplemented with 10% fetal bovine serum (FBS), 1% L-glutamine, and 1% penicillin/streptomycin, under standard conditions of 37 °C in a humidified atmosphere containing 5% CO_2**.**

Table 1. *Stable cell lines established using CRISPR-Cas9 system.*

Cell line	Aplication
DNMT3A-THP1-_KO2	Gene and protein expression analysis mRNA expression qRT-PCR
DNMT3A-THP1-_KO4	

3.2. Material

3.2.1. Oligonucleotides

Table 2. *Oligonucleotides used in this thesis.*

Name	Sequence (5' -> 3')	Application
5780 c.786T>A_template	AGCCCACTGACCCCGCATCCCCCACTGTGGCTACCACGCCAGAGCCCGTGGGGTCCGATGCTGGGGACAAGAATGCCACC	Nucleofection
5781 c.729C>T_template	AATGAATGCTGTGGAAGAAAACCAGGGGCCCGGGGAGTCTCAGAAGGTGGAGGAGGCCAGTCCTCCTGCTGTGCAGCAGCC	Nucleofection
5782 c.759C>T_template	GCCCACTGACCCTGCATCCCCCACTGTGGCTACCACGCCTGAGCCCGTGGGGTCCGATGCTGGGGACAAGAATGCCACCAAA	Nucleofection
5783 c.741G>A_template	ATGAATGCTGTGGAAGAAAACCAGGGGCCCGGGGAGTCTCAGAAGGTGGAGGAGGCCAGCCCTCCTGCTGTACAGCAGCCCACTGA	Nucleofection
5786 c.786T_template	AGCCCACTGACCCCGCATCCCCCACTGTGGCTACCACGCCTGAGCCCGTGGGGTCCGATGCTGGGGACAAGAATGCCACC	Nucleofection

5787 c.729C_template	AATGAATGCTGTGGAAGAAAACCAGGGGCCCGGGGAGTCTCAGAAGGTGGAGGAGGCCAGCCCTCCTGCTGTGCAGCAGCC	Nucleofection
5788 c.759C_template	GCCCACTGACCCCGCATCCCCCACTGTGGCTACCACGCCTGAGCCCGTGGGGTCCGATGCTGGGGACAAGAATGCCACCAAA	Nucleofection
5789 c.741G_template	ATGAATGCTGTGGAAGAAAACCAGGGGCCCGGGGAGTCTCAGAAGGTGGAGGAGGCCAGCCCTCCTGCTGTGCAGCAGCCCACTGA	Nucleofection
CD.Cas9.MZBL2518.AA	mG*mC*mU* rArCrC rArCrG rCrCrU rGrArG rCrCrC rGrUrG rUrUrU rUrArG rArGrC rUrArG rArArA rUrArG rCrArA rGrUrU rArArA rArUrA rArGrG rCrUrA rGrUrC rCrGrU rUrArU rCrArA rCrUrU rGrArA rArArA rGrUrG rGrCrA rCrCrG rArGrU rCrGrG rUrGrC mU*mU*mU* rU	CRISPR-Cas9
CD.Cas9.MZBL2518.AL	mC*mU*mC* rCrArC rCrUrU rCrUrG rArGrA rCrUrC rCrCrG rUrUrU rUrArG rArGrC rUrArG rArArA rUrArG rCrArA rGrUrU rArArA rArUrA rArGrG rCrUrA rGrUrC rCrGrU rUrArU rCrArA rCrUrU rGrArA rArArA rGrUrG rGrCrA rCrCrG rArGrU rCrGrG rUrGrC mU*mU*mU* rU	CRISPR-Cas9

3.2.2. Constructs

Table 3. *Constructs used in this thesis.*

Constructs	Identifier
WT DNMT3A	5563
507 G>A	5564
561 G>A	5565
729 C>T	5566
732del	5567
741 G>A	5568
752del	5569
753 T>C	5570
759 C>T	5571
840 C>T	5572
1131 C>T	5573
2013 G>A	5574
2412 G>A	5575

3.2.3. Media and Solutions

Table 4. *Media and solutions used in this thesis.*

Media/Solution	Source/Manufacture	Application
RPMI 1640	Gibco™	cell culture media
Dublecco's PBS	Gibco™	cell culture applications
Fetal Calf Serum (FCS)	-	cell culture media ingredient
L-glutamine	-	cell culture media ingredient
Penicillin/ Streptomycin	OS-B, Capricorn	cell culture antibiotics
TAE Buffer	40 mM Tris, 20 mM acetic acid, 1 mM EDTA	agarose gel electrophoresis
Cell Lytic M Buffer	Sigma Aldrich	Cell Lysis
SDS Lysis Buffer	Made in the lab	Cell Lysis
Cryo Media	% FBS (v/v), 10 % DMSO (v/v)	Cryo Conservation of cells

3.2.4. Antibodies

Table 5. *Antibodies used in this thesis.*

Antibody	Source	Identifier
DNMT3A (D23G1) Rabbit, monoclonal antibody (1:20 WES)	Cell Signaling Technology	Cell Signaling Technology #3598
DNMT3A Isoform 2 (E1Y50) Rabbit, monoclonal antibody (1:20 WES)	Cell Signaling Technology	Cell Signaling Technology #44807
DNMT3A (E9P2F) Rabbit, monoclonal antibody (1:20 WES)	Cell Signaling Technology	Cell Signaling Technology #49768
a-Tubulin ((11H10) Rabbit, monoclonal antibody (1:200 WES)	Cell Signaling Technology	Cell Signaling Technology #2125

3.2.5. Chemicals

Table 6. *Chemicals used in this thesis.*

Chemical	Source	Identifier
Nocodazole	STEMCELL Technologies	Catalog #74072
DMSO	Panreac Applichem	
Actinomycin D	Roth	8969,1
Reverse Transcriptase	Thermo Scientific	EP0452
RNase H	BioLabs	10250970
dNTP	Thermo Scientific	R0192
DTT	Invitrogen	D1532
Agarose	VWR	97062
Proteinase K	-	-
Ethanol	-	-
Alt-R HDR EnhancerV2	IDT	10007910
Eletroporation Enhancer	IDT	1075916
Cas9-GFP	IDT	10008161
Cas9-RFP	IDT	10008163
Nucleofection Buffer	Lonza	V4XC-3032
2x NebNext PCR master mix	NEB	M0541L

3.2.6. Commercial essays and kits

Table 7. *Commercial essays and kits used in this thesis.*

Assay/Kit	Source	Identifier
SG Cell Line 4D-Nucleofector™ X Kit S	Lonza	V4XC-3032
NucleoSpin Gel and PCR Clean-up	MACHEREY-NAGEL	REF 740609.50
QIAamp DNA Mini Kit	Quiagen	Quiagen 51304
Qubit dsDNA HS D1000	Thermo Fischer	Thermo Fischer
WES	Simple Protein	SM-W004
RevertAid H Minus First Strand cDNA synthesis Kit	Thermo Scientific/Invitrogen	K1632
RNeasy Micro Kit	Qiagen	217084
Qubit HS RNA	Agilent	Q32852
PierceTM BCA Protein Assay	Thermo Scientific	23227

3.2.7. Consumables

Table 8. *Consumables used in this thesis.*

Consumables	Source	Identifier
100 bp ladder	NEB	NEB N3231L
Cell Culture 6-well plates	Thermo Scientific	130184
Cell Culture 12-well plates	Thermo Scientific	130185
Cell Culture 24-well plates	Thermo Scientific	130186
Cell Culture 48-well plates	Thermo Scientific	130187
Cell Culture 96-well plates	Greiner Cellstar	650101
Low binding tubes	Eppendorf	EP0030108051
Reaction tubes 50 mL, 15 mL, 2 mL, 1.5 mL, 0.2 mL	Eppendorf	T8T8-500EA
qRT-PCR 96-well plates	ThermoFisher Scientific	AB0600
Adhesive sealing film for qRT-PCR	ThermoFisher Scientific	AB0558
Cryo tube for cell culture 2 mL	Saratedt	72.379
Pipette 5 mL, 10 mL, 25 mL	Sigma-Aldrich	Z331740

3.2.8. Devices

Table 9. *Devices used in this thesis.*

Devices	Source
PCR cycler	Applied Biosystems
Fluorescence microscope Observer Z1	Carl Zeiss
Heating block	Analytik Jena
NucleofectorTM 4D	Lonza
Different centrifuges	HettichLab
Laminar flow bench SterilGard	Thermo Scientific
TC10TM Automated Cell Counter	ThermoFisher

Qubit	Invitrogen
TapeStation 2200	Agilent
WES	ProteinSimple
QuantStudio qPCR	ThermoFisher
FACS Fortessa	BD Biosciences
FACS Aria	BD Biosciences
Balance	VWR
Cell Incubator	Thermo Scientific
Light Microscope	NIKON
Ice Machine	Hoshizaki
Fluorescence microscope Observer Z1	Zeiss
Sonicator	Bandelin
Vacuum pump VAC-MAN	Integra
Vortexer	Scientific industries
Water bath	GFL

3.2.9. Software

Table 10. *Software used in this thesis.*

Software	**Source**
SnapGene Viewer	SnapGene Software
AxioVision	Carl Zeiss Microscopy
Compass dor SW	Compass Software
FlowJo	FlowJo Software
Tape Station Analysis	Agilent
QuantStudio	Thermofisher
Graphpad Prism 7.01	GraphPad Software

Microsoft Office 365®	Microsoft
IGV	Open source
AI	Chatgpt and Perplexity

3.3. Methods

3.3.1. Cellular Methods

3.3.1.1. Cell culture

THP-1 cells were cultured under sterile conditions at 37°C in an environment with 5% CO_2 and 95% relative humidity. The cells were maintained as a suspension culture in RPMI-1640 medium supplemented with 10% fetal calf serum (FCS), 1% L-glutamine, and 1% penicillin-streptomycin, with the medium preheated to 37°C before use. Cell counting was performed using the TC10™ Automated Cell Counter following Trypan blue staining. To ensure optimal growth conditions, the cells were subcultured three times per week at a 1:10 ratio, maintaining a density of approximately 0.2–1 × 10^6 cells/mL.

1.1.1.1. Cell Lysate Preparation with SDS lysis buffer

Cell lysates were prepared using an SDS-based lysis buffer to ensure complete disruption of cellular membranes and efficient solubilization of total protein. A total of 4 × 10^6 cells per sample were harvested, washed once with cold PBS, and resuspended in 100 µL of SDS lysis buffer (10% SDS, 100 mM Tris-HCl pH 8.0, 150 mM NaCl, 10 mM EDTA pH 8.0). Following buffer addition, samples were sonicated on ice using a probe sonicator for 30 seconds per cycle, repeated 5 times at 45% amplitude, and the entire process was conducted twice to ensure complete lysis. The resulting lysates were centrifuged at 15,000 rpm for 3 minutes at room temperature to remove debris. Supernatants were collected and stored at −80 °C until use.

1.1.1.2. Cell Lysate Preparation with Cell Lytic M reagent

Cell lysates were prepared using Cell Lytic M buffer (Sigma-Aldrich) to extract soluble proteins under non-denaturing conditions. A total of 2 × 10^6 cells per sample were harvested, washed once with cold PBS, and resuspended in 125 µL of Cell Lytic M buffer. Samples were incubated on a shaker at 500 rpm for 15 minutes at room temperature to allow thorough lysis. Following incubation, lysates were centrifuged at 18,000 × g for 15 minutes at 4 °C to remove cell debris. Supernatants were collected and stored at −80 °C until further use.

1.1.1.3. Electroporation of THP-1 cells

THP-1 cells were electroporated using the Lonza Nucleofector™ 4D device with the Lonza Kit SG (V4SC-3096)**.** Ribonucleoprotein (RNP) complexes were first assembled by combining Cas9-RFP (52 µM) and synthetic

gRNA (targeting DNMT3A; 50 µM) at a 1:1.5 molar ratio. Each RNP preparation was incubated for 10 minutes at room temperature to allow complex formation. The nucleofection mixture was composed of the RNP complex, 100 µM electroporation enhancer (IDT), and 100 mM HDR donor oligonucleotides, which contained the desired point mutation flanked by homologous arms. THP-1 cells were resuspended in SG buffer at a density of 2×10^5 cells per nucleofection cuvette (16-well strip format) or 1×10^6 cells per vessel (larger-scale format). The total reaction volume was adjusted with PBS to reach the final volume as specified by the manufacturer. Electroporation was carried out using the FF-100 program, optimized for THP-1 cells, following the standard Lonza protocol. Post-nucleofection, cells were immediately transferred into pre-warmed complete RPMI 1640 medium and incubated under standard culture conditions (37 °C, 5% CO_2).

Post-nucleofection, cells in 96-well strips were maintained in complete RPMI-1640 medium supplemented with 690 µM HDR enhancer (IDT), while negative-control samples received an equivalent volume of DMSO. Larger-format cultures were maintained in 12-well plates under identical supplementation conditions. After 24 hours, all cultures were refreshed with standard RPMI-1640 medium supplemented with 10% FBS, L-glutamine, and antibiotics to ensure optimal cell recovery and continued growth.

1.1.1.4. Fluorescence microscopy

The fluorescence microscope Observer Z1 (Carl Zeiss) was used for microscopic imaging. GFP signals were excited at 483 nm with an emission maximum of 506 nm and detected using a GFP HC filter. Cy3 and mCherry signals were excited at 550 nm and 587 nm, respectively, with emission maxima at 570 nm and 610 nm, and were detected using a Cy3 filter.

1.1.1.5. Flow Cytometry

To assess nucleofection efficiency, flow cytometry was performed using the BDLSRFortessa flow-cytometer. RFP-positive cells were detected using the G-582-15-A laser, while GFP detection was performed with the B-530-30-A laser. To ensure accurate analysis, cells of interest were initially identified and gated based on forward scatter area (FSC-A) and side scatter area (SSC-A) parameters, enabling exclusion of subcellular debris and non-viable particulate material from subsequent analyses, followed by singlet selection based on forward scatter height (FSC-H) and forward scatter area (FSC-A) to exclude multiplets. Fluorescence-based gating was then applied to distinguish four populations: GFP^-/RFP^-, GFP^+/RFP^-, GFP^-/RFP^+, and GFP^+/RFP^+.

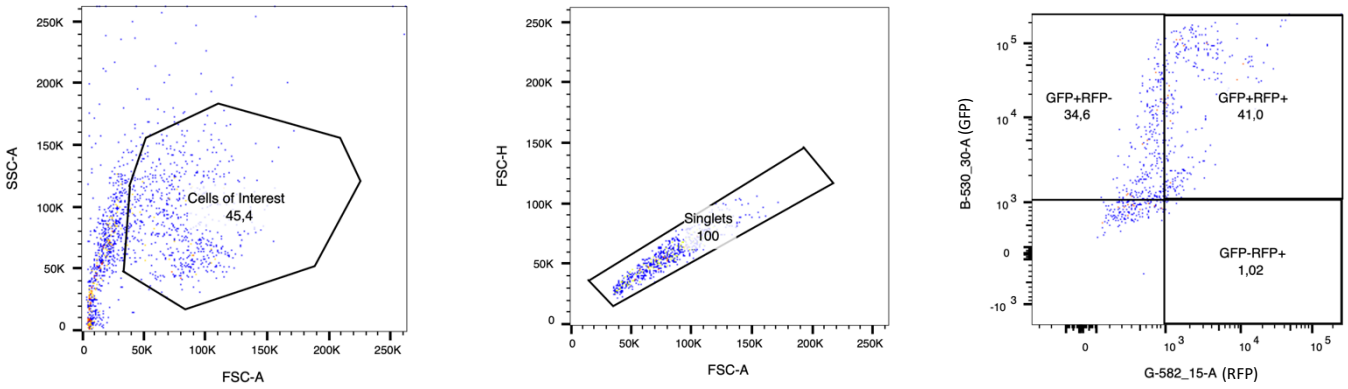

Figure 5. Flow cytometry-based gating strategy for identification of double-positive and single-positive populations. FACS data from a positive control Cas9-RFP and FITC labeled gRNA.

After approximately 50 hours, the FACS ARIA was used to sort RFP-positive cells, maintaining the same laser configurations and gating strategy for consistency. Sorting was performed as index single-cell index sorting into 96-well plates, enabling precise isolation of successfully nucleofected cells for downstream analysis. The means and standard errors were calculated and statistical significance was determined using the Friedman's and Krustal-Wallis tests.

1.1.1.6. Proliferation Assay

To evaluate cell proliferation and determine population doubling time, 10,000 cells per condition were seeded in 48-well plates in triplicate. Cell growth was monitored over a period of three weeks, with cell counts performed every 48 hours using an automatic cell counter to ensure consistent and unbiased quantification of cell number. As cultures reached optimal cell density, cells were sequentially expanded to larger vessels, first into 24-well plates, then 12-well, and eventually into 6-well plates, to prevent overgrowth and maintain optimal growth conditions. At each passage, cells were resuspended, centrifuged at 300 × g for 5 minutes, and reseeded at a consistent density to preserve continuity in cell growth evaluation.

This passaging strategy enabled accurate tracking of cumulative cell proliferation over time. Cell counts obtained at each 48-hour interval were used to calculate growth curves and assess population doubling time under each experimental condition (Kimiz-Gebologlu et al., 2022).

$$Doubling\ Time\ (days) = \frac{2 \text{ x } \ln(2)}{\ln(\frac{Cell\ number\ at\ start}{Cell\ number\ at\ x\ timepoint})}$$

3.3.2. Molecular Methods

3.3.2.1. Sanger Sequencing

Genomic DNA (gDNA) was extracted from THP-1 CRISPR-edited cells using the QIAamp DNA Mini Kit (Qiagen) according to the manufacturer's protocol. DNA concentration and purity were assessed using a Qubit fluorometer (Thermo Fisher Scientific) with the Qubit dsDNA HS Assay Kit to ensure accurate quantification. For PCR amplification, the NEBNext 2X PCR Master Mix (New England Biolabs) was used in a total reaction volume of 30 µL. Each reaction contained 2 ng of gDNA, 15 µL of NEBNext 2X PCR Master Mix, and 1 µL of each primer (forward and reverse) at a concentration of 25 µM. The target amplicon was 467 bp in length with a GC content of 64%, and primers had a melting temperature of 59ºC. The following PCR program was used: an initial denaturation at 98ºC for 30 seconds, followed by 35 cycles of denaturation at 98ºC for 10 seconds, annealing at 62ºC for 30 seconds, and extension at 72ºC for 30 seconds. A final extension step was performed at 72ºC for 2 minutes, and reactions were held at 4ºC until further processing. Following amplification, PCR products were analyzed via 1.5% agarose gel electrophoresis. Samples were loaded onto a gel prepared in 1X TAE buffer and stained with HDGreen. A 100 bp DNA ladder was used as a molecular weight reference, and electrophoresis was carried out at 80 V for 1 hour and 30 minutes. Bands were visualized under UV illumination using a Bio-Rad imager. PCR products were then purified using the NucleoSpin Gel and PCR Clean-up Kit (Macherey-Nagel) following the manufacturer's instructions. The purified DNA was eluted in 15 µL of elution buffer and quantified using a Qubit fluorometer. Samples were subsequently sent for Sanger sequencing using both forward and reverse primers. Resulting chromatograms were analyzed with SnapGene to confirm the sequence and identify any mutations.

3.3.2.2. Protein quantification by BCA

Protein concentration was quantified using the Pierce BCA Protein Assay Kit, according to the manufacturer's instructions for the microplate format. Samples were prepared using SDS-containing lysis buffer to ensure complete solubilization of membrane-bound and cytoplasmic proteins. Standards and samples were incubated with the working reagent (a 50:1 mixture of Reagent A and Reagent B) in a 96-well plate, with a total reaction volume of 200 µL per well. The plate was incubated at 37°C for 30 minutes to allow for color development, and absorbance was measured at 562 nm using a microplate reader. Protein concentrations were calculated based on a standard curve, which included the following concentrations: 0, 125 µg/mL, 250 µg/mL, 500 µg/mL, 750 µg/mL, 1000 µg/mL, 1500 µg/mL, and 2000 µg/mL, generated with serial dilutions of bovine serum albumin (BSA). To ensure accuracy and reproducibility, all measurements were performed in technical duplicates.

3.3.2.3. Protein expression analysis using WES

WES was employed to quantify protein levels in indel-containing knockout cell lines, generated using CRISPR-Cas9 technology. The analysis was conducted using the 12–230 kDa kit, with the following parameters: separation time of 25 minutes, separation voltage of 375 volts, antibody diluent incubation for 5 minutes, primary antibody incubation for 60 minutes, and secondary antibody incubation for 30 minutes. Cell lysates were prepared using SDS lysis buffer to ensure optimal protein extraction. Protein detection focused specifically on DNMT3A isoform 1, the isoform of interest in this study, and α-tubulin was used as a loading control for normalization. As controls, HEK293A wild-type (WT) cells, DNMT3A-overexpressing cells, and input $CD34^+$ cells were included to facilitate accurate quantification and comparative analysis of protein expression levels.

3.3.2.4. DNMT Activity Assay

The DNMT Activity Quantification Kit (Colorimetric) (Abcam, ab113467) was used to assess DNA methyltransferase (DNMT) activity in the KO lysates prepared with Cell Lytic M lysis reagent, to maintain the integrity and activity of the cells. The assay is based on the capture of methylated DNA by an immobilized substrate, followed by colorimetric detection using specific antibodies.

A total of 10 µg of lysate was used per reaction well, in accordance with the manufacturer's instructions. The assay was conducted in a 96-well strip plate format, and the following parameters were applied: enzymatic incubation at 37 °C for 120 minutes, followed by sequential antibody incubations, capture antibody for 60 minutes, detection antibody for 30 minutes, and enhancer solution for 30 minutes. Each antibody incubation step was followed by three washes with 1× wash buffer to minimize background signal. Color development was achieved by adding developer solution and incubating for up to 10 minutes before the addition of stop solution. Absorbance was measured at 450 nm using a microplate reader. All experimental samples were run in technical duplicates, and each assay plate included a blank and a positive control (provided by the kit).
The enzymatic activity was subsequently expressed as OD per hour per milligram of protein (OD/h/mg).

$$DNMT\ activity\ (OD/h)/mg) = \frac{(\text{Sample OD} - \text{Blank OD})}{(\text{Protein Amount } (\mu g) x\ hour)}$$

3.3.2.5. Transgene Overexpression and mRNA stability assay via Actinomycin D Time-Course

To evaluate the post-transcriptional effects of DNMT3A synonymous mutations on mRNA stability, CRISPR-Cas9-generated DNMT3A knockout (KO) THP-1 cell lines were transfected with a panel of 13 pre-cloned DNMT3A expression constructs. These included wild-type (WT), synonymous mutant, and deletion variants previously available in the laboratory. Nucleofection was performed using the Lonza 4D-Nucleofector™

system and SG Cell Line 4D-Nucleofector™ X Kit in nucleofection strips, following the manufacturer's instructions. Each nucleofection reaction used 2×10^5 cells and 0.1 µg of plasmid DNA, employing the FF-100 program optimized for THP-1 cells. After transfection, cells were cultured in complete RPMI-1640 medium at 37 °C with 5% CO_2 for 48 hours to allow for expression.

To assess mRNA stability, transcription was halted using Actinomycin D (5 µg/mL final concentration), and cells were harvested at seven distinct time points: 0 h (no treatment), 30 min, 1 h, 2 h, 4 h, 8 h, and 24 h post-treatment. At each time point, cells were pelleted by centrifugation at 400 × g for 5 minutes at 4 °C, washed with cold PBS, and stored at –80 °C until RNA extraction.

Total RNA was extracted using the RNeasy Micro Kit, and RNA concentration and quality were assessed using the Qubit™ RNA HS Assay Kit (Thermo Fisher Scientific) and the Agilent TapeStation System. Only samples with RNA integrity numbers (RIN) ≥ 6 were used for downstream analysis. cDNA synthesis was performed with the RevertAid H Minus First Strand cDNA Synthesis Kit (Thermo Scientific), following the manufacturer's instructions. The resulting cDNA was diluted 1:5 with nuclease-free water for subsequent analysis.

Quantitative PCR (qPCR) was conducted using TaqMan™ Gene Expression Assays (Applied Biosystems) on the QuantStudio™ 6 Flex Real-Time PCR System. Each reaction (20 µL) contained 10 µL of TaqMan™ Universal PCR Master Mix, 1 µL of the specific TaqMan probe, 4 µL of diluted cDNA 400ng, and nuclease-free water. All reactions were run in technical triplicates. Gene expression was normalized to RPL37A, and mRNA half-lives were calculated using the ΔCt values relative to time point 30min. Data were analyzed to compare mRNA decay kinetics between WT, synonymous, and deletion constructs.

3.3.3. Statistical data analysis

Statistical tests were conducted utilizing GraphPad Prism 7.01. Normality tests were conducted to determine the appropriate statistical approach, and either parametric or non-parametric tests were applied accordingly, as specified in the figure legends. The level of significance was denoted by asterisks corresponding to the following p-values: ns = $p > 0.05$; * = $p \leq 0.05$; ** = $p \leq 0.01$; *** = $p \leq 0.001$; **** = $p \leq 0.0001$.

4. Results

4.1. CRISPR-Cas9 Editing and Nucleofection Efficiency

To optimize nucleofection conditions for efficient delivery of CRISPR/Cas9 components into THP-1 cells, the uptake of oligonucleotides with and without FITC labelling was initially assessed. The flow cytometry data revealed three main populations: $GFP^{-}RFP^{+}$ (Cas9 only), $GFP^{+}RFP^{+}$ (co-delivery), and $GFP^{+}RFP^{-}$ (FITC oligos only). In **Figure 6a**, where FITC-labeled donor oligonucleotides were employed, both AA1 and AA2 displayed a predominant population of GFP^{+}/RFP^{-} (AA1 mean= 80.70±12.758; AA2 mean = 3.635±5.141) cells, consistent with the uptake of the donor oligos as detected by the FITC signal alone. The GFP^{+}/RFP^{+} (AA1 mean = 14.0±5.515; AA2 mean = 14.750±5.869) double-positive population was present but remained relatively modest in both cell types, while GFP^{-}/RFP^{+} (AA2 mean = 3.635±5.141) events were negligible, indicating minimal Cas9-RFP uptake without concurrent donor detection. This pattern demonstrates that FITC labeling itself does not interfere with Cas9-RFP uptake or co-delivery, although it also highlights that RNP delivery efficiency was suboptimal in a subset of cells. Notably, AA1 exhibited a higher proportion of GFP^{+}/RFP^{+} cells compared to AA2, suggesting more efficient simultaneous donor uptake and Cas9 delivery in AA1 under FITC-labeled conditions. In **Figure 6b**, using non-labeled donor oligonucleotides, the expected distribution shifted: both AA1 and AA2 exhibited detectable GFP^{-}/RFP^{+} (AA1 mean= 10.885±2.567; AA2 mean= 18.0±1.980) populations, reflecting successful Cas9-RFP delivery, while GFP^{+}/RFP^{-} and GFP^{+}/RFP^{+} events were absent because no FITC signal was present. The relative proportions indicate that AA1 again outperformed AA2, showing a larger GFP^{-}/RFP^{+} fraction and therefore a higher baseline efficiency of RNP delivery in the absence of donor labeling. Collectively, these findings confirm that donor oligo uptake is not the primary limiting factor in this system, rather, the efficiency of Cas9-RFP delivery dictates overall editing outcomes. The modest GFP^{+}/RFP^{+} frequencies observed in **Figure 6a** indicate that the presence of FITC on the donor oligos does not interfere with Cas9–RNP delivery or its cellular uptake, as the RNP complexes themselves are unlabeled. This comparison is presented to show that, although FITC labeling could theoretically affect cell survival, particularly if FITC-tagged donors were incorporated into the genome during homology-directed repair, it does not measurably hinder the co-delivery process itself. Rather, it highlights that differences in GFP^{+}/RFP^{+} frequencies primarily reflect RNP delivery efficiency rather than any intrinsic barrier imposed by FITC labeling. However, qualitative inspection suggested a slight reduction in cell viability under FITC-labeled conditions, potentially attributable to fluorophore-related cytotoxicity or post-nucleofection stress. However, this observation was not quantified or documented. Importantly, across both experimental conditions, AA1 consistently exhibited superior co-delivery and editing-related fluorescence profiles compared to AA2, indicating that AA1 is intrinsically more amenable to efficient RNP uptake and functional integration of donor oligonucleotides.

In vitro cleavage assays were performed using TapeStation analysis to assess the functionality of two guide RNAs, AA and AL. As shown in **Figure 6c**, the cleavage products are visible as distinct bands, with the thickest lines representing the expected cut sites generated by Cas9-mediated DNA cleavage. A comparison between expected and observed fragment sizes confirmed that cleavage occurred at or near the predicted target sites. For gRNA AA, cut 1 was expected to yield fragments of 124 bp and 118 bp, and cut 2 fragments of 343 bp and 279 bp, the observed bands matched these sizes closely. For gRNA AL, expected fragment sizes were 397 bp (cut 1) and 467 bp (cut 2), with observed bands at 354 bp and 423 bp, respectively (**Figure 6d**). While the TapeStation provides semi-quantitative and higher-resolution results compared to other methods, the detected patterns strongly support the specific and efficient cleavage activity of both guide RNAs.

After, three nucleofection programs, FF100 (the standard for THP-1 cells), DK100 (reported by Lonza to enhance transfection efficiency), and CM138 (designed to maximize cell viability) were compared in order to optimize delivery conditions for Cas9-RFP. Cas9-RFP delivery efficiency was calculated as the percentage of RFP-positive cells among total singlets. As shown in **Figure 6e**, FF100 (first two samples) resulted in transfection efficiencies of approximately 55% and 58% at 50 hours (grey points) and maintained acceptable cell survival throughout the culture period, although this observation was not quantified or documented. DK100 (next two samples) produced slightly lower transfection efficiencies of 26% and 11% at the 20 h timepoint, which further declined to 7% at 50 h. Notably, this reduction appeared to coincide with increased cell death observed during routine microscopic inspection post-nucleofection, although cell viability was not quantitatively assessed. In contrast, CM138 (final two samples) yielded the highest cell survival, with cells appearing healthy and robust in culture, but transfection efficiencies were substantially lower, at 5% and 2% at 20h and having a slight increase to 12% and 9% at 50 hours, respectively. Based on these results, FF100 was selected as the optimal nucleofection program for subsequent experiments, as it provided the best compromise between efficient gene delivery and cell survival.

It should be emphasized that no clear differences can be discerned from the current data. Therefore, these findings must be regarded as preliminary observations that require replication and rigorous statistical validation before any definitive conclusions can be drawn.

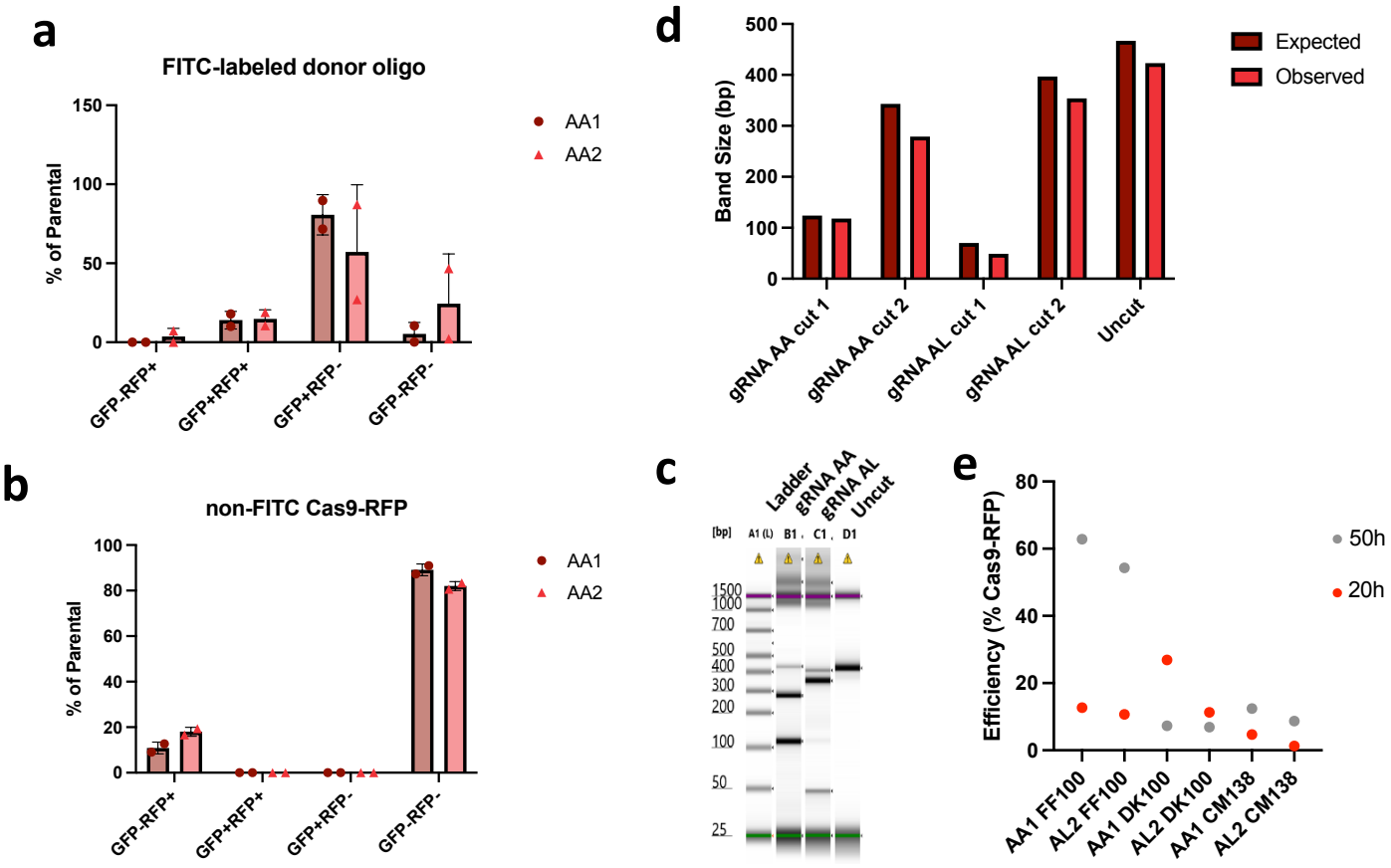

Figure 6. Optimization of THP-1 Nucleofection. a Distribution of THP-1 cell populations after nucleofection with FITC-labeled donor oligonucleotides. Values are represented as mean ± SD. Normalization was performed prior to analysis, and a non-parametric one-way ANOVA was conducted using Friedman's test followed by Dunn's multiple comparisons test, where significance was not reached due to insufficient statistical power resulting from a lack of biological replicates. **b.** Distribution of THP-1 cell populations after nucleofection with non-FITC labeled oligonucleotides and Cas9-RFP. Normalization was performed, and non-parametrical ANOVA was applied using the Krustal-Wallis test, followed by multiple comparisons, where statistical significance could not be established owing to limited statistical power, primarily attributable to an insufficient number of biological replicates. **c.** TapeStation gel image showing DNA fragment sizes for different gRNA conditions. Lanes correspond to the DNA ladder, uncut control (U), and samples digested with gRNAs (gRNA AA and gRNA AL). **d.** Comparison of expected vs. observed fragment sizes obtained from TapeStation analysis, where the analysis did not achieve significance because the dataset lacked adequate biological replication to provide sufficient statistical power. **e.** Impact of different nucleofection programs on efficiency over time, 20h black circles and 50h grey circles, where significance was not attained, likely reflecting reduced statistical power stemming from the low number of biological replicates available.

4.2. Generation of DNMT3A KO THP-1 cell culture models

Stable cell lines with a DNMT3A knockout were established using an electroporation system. Oligonucleotides harboring either wild-type (WT) or synonymous mutations, c.786T>A, c.729C>T, c.759C>T, c.741G>A, as well as their corresponding WT sequences (c.786T, c.729C, c.759C, c.741G), were designed and synthesized by Dr. Marius Kulp. THP-1 cells were nucleofected with RNP complexes comprising RFP-tagged Cas9, guide RNA (gRNA-AA or gRNA-AL) (**Figure 7a,b,c**), and a pair of single-stranded oligonucleotides (one WT and one mutated). This setup enabled targeted double-strand breaks (DSBs) and subsequent integration

via homology-directed repair (HDR). The inclusion of RFP-tagged Cas9 allowed real-time tracking and fluorescence-activated cell sorting (FACS)-based selection of successfully nucleofected cells.

To confirm successful editing and enrichment of modified cells, fluorescence-activated cell sorting (FACS) was performed 48 hours after nucleofection, during which RFP^+ cells were initially enriched. These sorted populations were subsequently subjected to single-cell sorting to establish individual clonal cultures. The resulting clones were expanded over two weeks, and genomic DNA was extracted for Sanger sequencing to verify precise oligonucleotide incorporation. Although homology-directed repair (HDR) was the intended repair mechanism, sequencing revealed a high frequency of insertions and deletions (InDels) at the target site, indicating predominant repair via non-homologous end joining (NHEJ), a phenomenon extensively reported in THP-1 and other myeloid cell lines (Pinaud & Zamborlini, 2025). Clones harboring InDels consistent with gene disruption were selected for further analysis. Importantly, Sanger sequencing demonstrated no detectable differences in the distribution of cleavage sites between the two gRNAs (AA1 and AA2) in both cases, the majority of InDels clustered near position 11 (~32%) relative to the gRNA PAM, with secondary cleavage hotspots observed at positions −3 and 12 (~18%), reflecting a reproducible, non-random CRISPR cleavage pattern (**Figure 7d**).

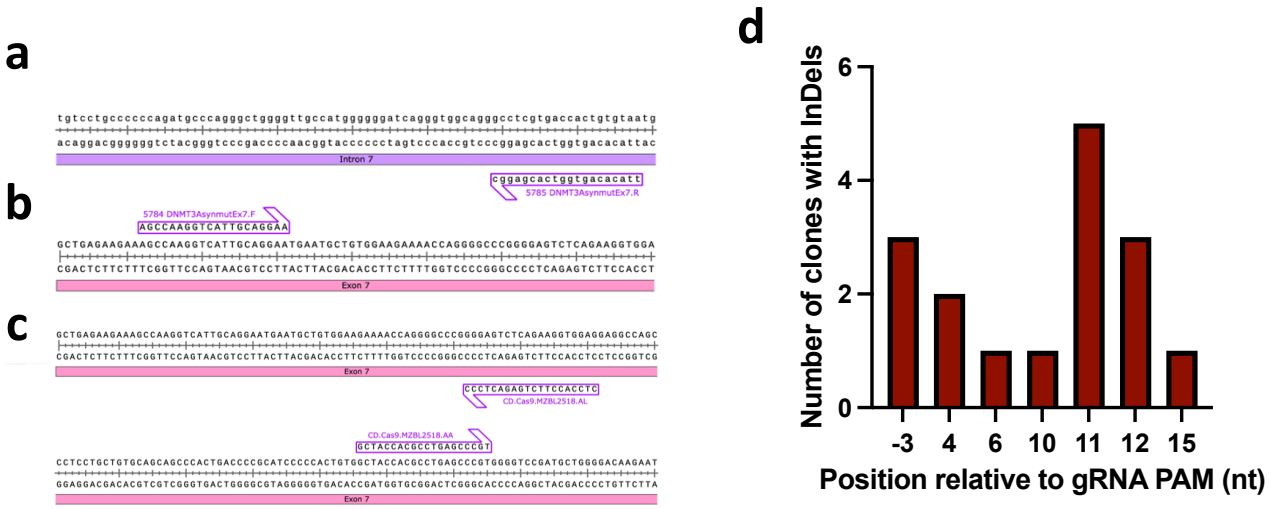

Figure 7. Mapping of CRISPR editing sites and distribution of indel formation in DNMT3A exon 7. a. Schematic representation of intron 7 with the positions of primer 5785 DNMT3AsymmutEx7.R used for amplification, indicated by an arrow. **b.** Sequence view of the 5′ region of exon 7 showing the forward primer binding site (5784 DNMT3AsymmutEx7.F) used for amplification and sequencing. **c.** Sequence view of the target region within exon 7 showing the two gRNA binding sites, CD.Cas9.MZBL2518.AA and CD.Cas9.MZBL2518.AL are indicated. **d.** Histogram showing the distribution of insertion and deletion (indel) events relative to gRNA PAM (nt).

These CRISPR-induced knockout clones were further characterized using phenotypic and molecular assays. Morphologically, all DNMT3A knockout clones maintained the typical round, suspension-growing phenotype observed in wild-type THP-1 cells when inspected by light microscopy, these observations were qualitative and not documented with imaging. Functional growth analyses demonstrated that knockout lines

proliferated at rates comparable to wild-type cells. Mean live cell counts over a 15-day culture period revealed overlapping growth curves between wild-type and all six knockout clones, with no statistically significant differences in cell expansion (**Figure 8a**). Doubling time analysis demonstrated that DNMT3A knockout clones exhibited variable proliferation rates compared to THP-1 wildtype cells. The wildtype line showed a doubling time of approximately 48 hours, in agreement with the reference value reported by DSMZ for this cell line. In contrast, KO2 displayed a shorter doubling times, indicating accelerated proliferation relative to WT. Conversely, KO1, KO4, and KO6 exhibited prolonged doubling times, suggesting reduced proliferative capacity under the same conditions. Despite these trends, statistical analysis across three independent biological replicates revealed no significant differences in doubling time when comparing each knockout clone to the wildtype. The individual doubling times of each established clone, ranged from approximately 20 to 72 hours and are summarized in **Table 11**. Cell viability remained generally high over the 15-day monitoring period for both THP-1 wild-type and all knockout clones (KO1–KO6); however, notable transient deviations were observed. Most clones, including the wild-type, exhibited an initial drop of approximately 50 % in viability on day 2 (35-55% viability) before recovering to baseline levels. In addition, KO5 and KO6 displayed a secondary decline in viability around day 6 (41% viability), while KO2 showed a distinct reduction in viability at day 10 (50% viability). Despite these fluctuations, all cultures subsequently recovered, and no statistically significant differences in overall viability were detected between knockout and wild-type populations across the three biological replicates. (**Figure 8b**).

Table 11. *Characterization of the established cell lines.*

Cell Line	**Laboratory Designation**	**Morphology**	**Doubling time (h)**
THP-1	DSMZ wild-type	Small, round Suspension Cells	~48±3.529
	THP-1_DNMT3A_KO_1		~72±4.761
	THP-1_DNMT3A_KO_2		~50±3.877
	THP-1_DNMT3A_KO_3		~20±0.7847
	THP-1_DNMT3A_KO_4		~72±6.638
	THP-1_DNMT3A_KO_5		~43±3.510
	THP-1_DNMT3A_KO_6		~72±6.565

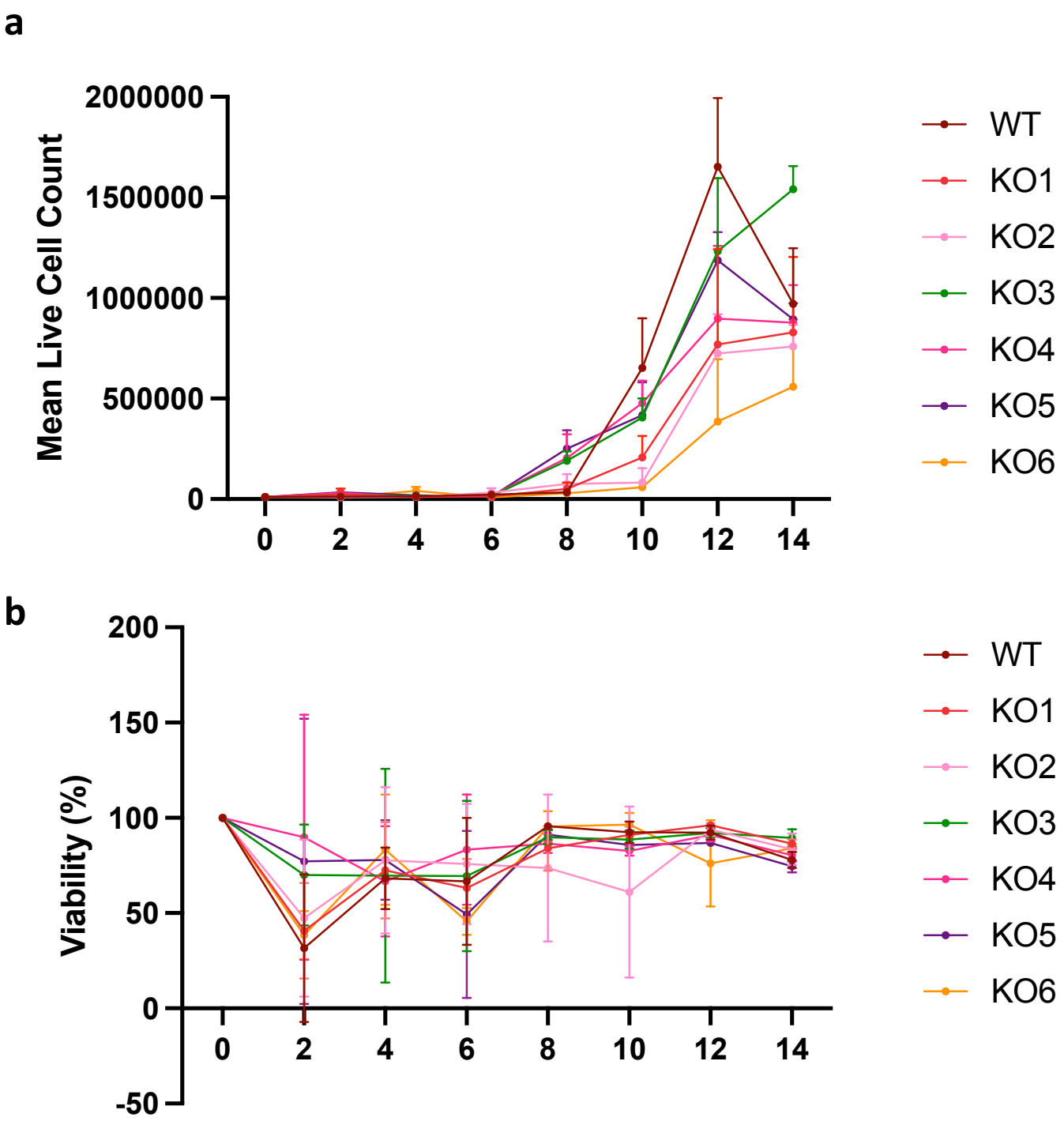

Figure 8. Growth and viability analysis of DNMT3A knockout clones compared to wild-type THP-1 cells. a. Proliferation curves showing mean live cell counts over a 14-day culture period for wild-type (WT) THP-1 cells and six independent DNMT3A knockout (KO) clones. Cell numbers were determined at regular intervals using trypan blue exclusion and quantified with an automated cell counter. Normalization was performed prior to analysis, and a non-parametric one-way ANOVA was conducted using Kruskal-Wallis test also for multiple comparisons, although statistical significance was not reached across the three independent biological replicates analyzed for each condition**. b.** Viability analysis expressed as the percentage of live cells over the 14-day monitoring period for WT and KO clones, showing stable viability across all groups. Normalization was performed prior to analysis, and a non-parametric one-way ANOVA was conducted using Kruskal-Wallis and Dunn's test for multiple comparisons, there was no statistical significance when comparing the KO to the WT.

To verify successful knockout at the protein level, a capillary-based Western blotting (WES) was employed. Protein lysates were prepared from THP-1 wild-type (WT) and knockout (KO) clones using SDS lysis buffer. In addition, lysates from HEK293T cells (both WT and DNMT3A-overexpressing) and from $CD34^+$ cells were included as controls, these control lysates had been previously generated using Cell Lytic M buffer. The $CD34^+$ samples represent primary hematopoietic stem and progenitor cells (HSCs), which naturally express DNMT3A and serve as a biologically relevant reference for endogenous DNMT3A expression and processing. Their inclusion as controls allowed comparison of DNMT3A levels in engineered THP-1 cells to those in unmodified primary hematopoietic cells, thereby providing a physiologically meaningful baseline for interpretation of the Western blot data. For comparative analysis, 4 µL of lysate, adjusted to equal protein amount 41.9 ng, was loaded onto the WES platform to eliminate signal variability due to unequal protein loading. This adjustment was necessary, as earlier experiments using volumetric loading failed to yield a consistent signal for DNMT3A isoform 1. As shown in **Figure 9a**, endogenous DNMT3A in THP-1 wild-type, HEK293T wild-type appeared near the ~118–130 kDa region. In contrast, the HEK293T overexpression sample exhibited a dominant DNMT3A band migrating at a higher apparent molecular weight, likely reflecting the presence of additional vector-derived sequences (e.g., epitope tags) or post-translational modifications associated with overexpression. Within the knockout panel, DNMT3A protein was undetectable in KO2, KO4 and KO5, confirming successful knockout at the translational level. Interestingly, residual DNMT3A signals in KO1, KO3, and KO6 were also detected at a higher apparent molecular weight compared to wild-type THP-1, suggesting the presence of altered DNMT3A isoforms or fusion products arising from in-frame editing events or aberrant splicing. The α-tubulin loading control bands were largely uniform across samples, although a slightly reduced intensity was observed in the THP-1 wild-type lysate relative to the nucleofected samples. As observed by the DNMT3A normalized to the housekeeping gene, α-tubulin, signal in **Figure 9b**, HEK293T show higher signals, as expected, especially for the overexpressing lysate, and knockouts 1,3 and 6 have comparable values to THP-1 wild-type, confirming the unsuccessful knockout.

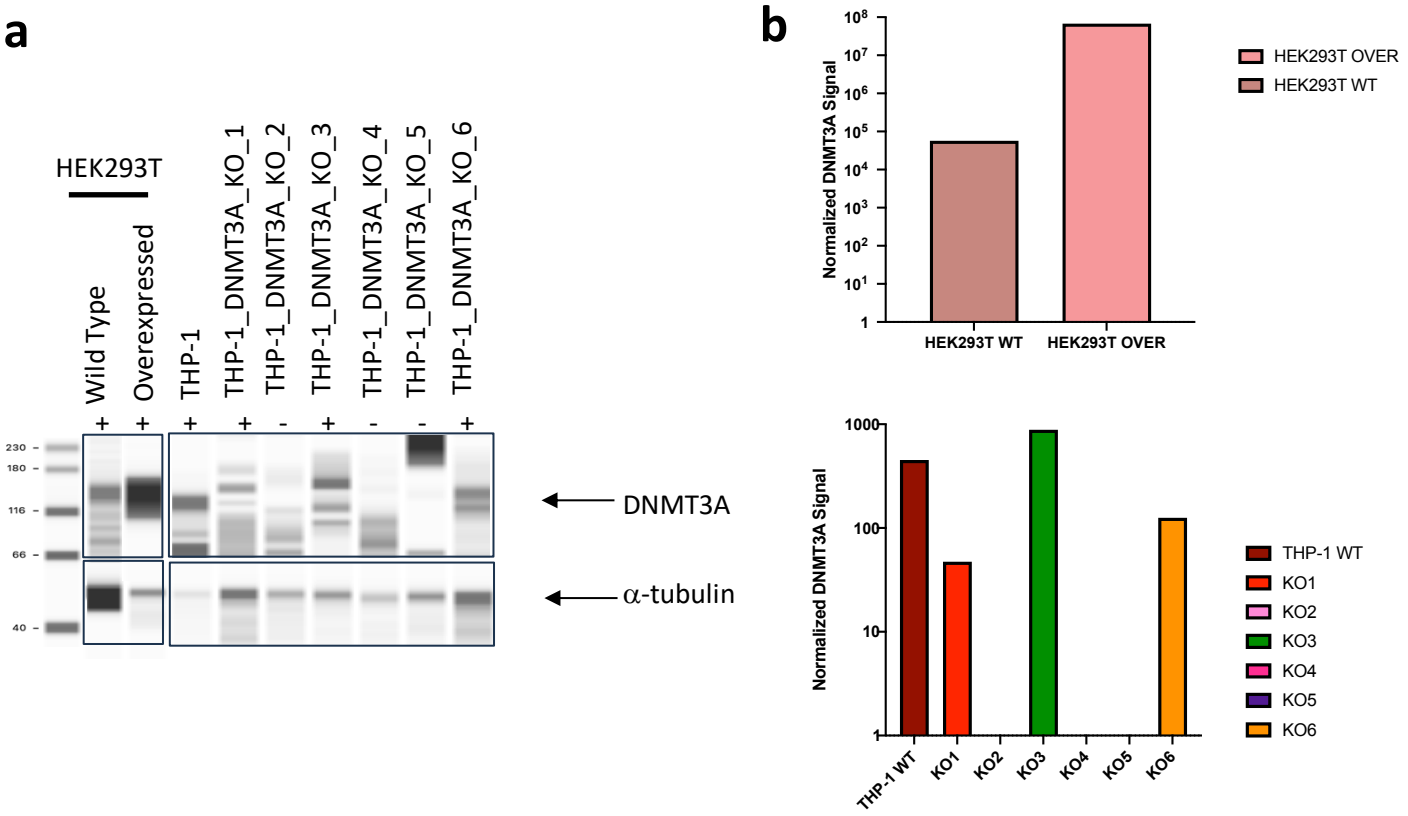

Figure 9. Validation of DNMT3A knockout at the protein level and assessment of residual DNMT enzymatic activity in THP-1 clones. **a.** Western blot analysis of DNMT3A protein expression in wild-type THP-1 cells, six independent DNMT3A knockout (KO) clones, and reference controls (HEK293T wild-type, HEK293T overexpressing DNMT3A, and CD34⁺ cells). α-tubulin was used as a loading control. Contrast was adjusted to each sample **b.** Lane normalization was performed according to AUC values of the housekeeping gene, α-tubulin, and normalization signals based on AUC of DNMT3A and lane normalization, for each sample, n=1.

Following confirmation of DNMT3A knockout at the protein level, overall DNMT enzymatic activity was quantified using a colorimetric DNMT activity assay to assess the functional impact of the knockout. Although this assay also detects residual activity from other isoforms such as DNMT1 and DNMT3B, it provides a robust proxy for total methyltransferase function. Each of the six knockout clones was analyzed in parallel with wild-type cells and enzymatic standards (0.5 µg and 1 µg DNMT control), and optical density (OD) values were normalized to the blank (OD = 0.22). As shown in **Figure 10**, wild-type THP-1 cells displayed strong DNMT activity, within the expected range of the positive controls, whereas all six knockout clones exhibited markedly diminished activity. KO3, KO4, and KO5 retained low but detectable residual activity consistent with near-complete loss of enzymatic function, while KO1, KO2, and KO6 showed increased activity levels, although not statistically relevant due to high standard deviation. Taken together with the WES data, these findings indicate that KO4 and KO5 are the most promising candidates for a complete DNMT3A knockout at both the protein expression and functional activity levels. However, these observations have not reached statistical significance and therefore require further verification through additional replicates and statistical analysis.

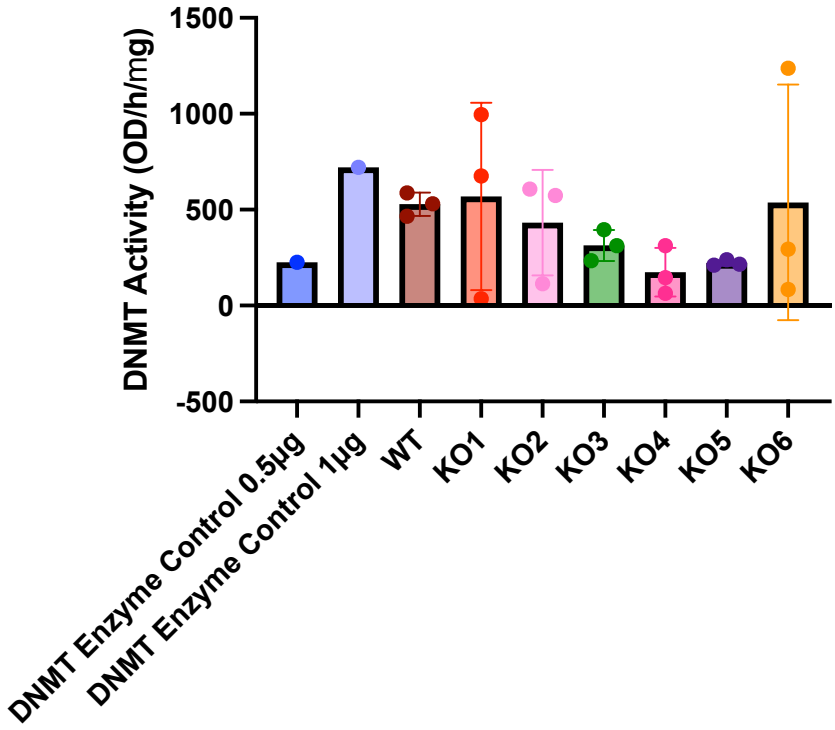

Figure 10. Quantification of total DNMT activity in wild-type THP-1 cells and DNMT3A KO clones using a colorimetric DNMT activity assay. Values (OD/h/mg) were normalized to blank readings and compared with DNMT enzyme standards (0.5 µg and 1 µg). Bars represent mean ± SD from independent replicates, with individual data points shown. Normalization was performed prior to analysis, and a non-parametric one-way ANOVA was conducted using Kruskal-Wallis test also for multiple comparisons, all comparisons are ns.

4.3. Development of Stable THP-1 Cell Models Carrying DNMT3A Synonymous Variants

To introduce patient-derived synonymous mutations into THP-1 cells, CRISPR-Cas9 ribonucleoprotein (RNP) complexes consisting of Cas9, gRNA-AA, and two single-stranded DNA oligonucleotides, one corresponding to the wild-type (WT) sequence and the other carrying either of the synonymous mutations: AA1 (c.786T>A) or AA2 (c.759C>T) were employed. This strategy, building on the well-established use of RNPs for genome editing to minimize off-target effects and transiently express Cas9, aimed to achieve monoallelic mutation through homology-directed repair (HDR). HDR is known to provide a high-fidelity mechanism for introducing precise genomic alterations but is inherently limited by its restriction to the S/G2 phases of the cell cycle.

To promote HDR, cells were treated with nocodazole (2 µg/µL), a microtubule-depolymerizing agent that arrests cells in G2/M phase. Prior studies have shown that synchronization of the cell cycle to enrich for G2/M populations can enhance the efficiency of HDR-mediated genome editing. Accordingly, four experimental conditions were established: AA1 + nocodazole, AA1, AA2 + nocodazole, and AA2. Following nucleofection, single-cell sorting was performed based on fluorescence markers. Wild-type cells were identified as RFP− singlets, whereas successfully nucleofected cells were sorted as RFP+, indicating the presence of Cas9-RFP fusion protein. Clonal populations were then expanded and analyzed by Sanger sequencing to evaluate

editing outcomes. Surprisingly, a reduction in clonogenic survival following single-cell sorting in nocodazole-treated groups, compared to untreated controls was observed (**Figure 11a**). This finding aligns with prior reports of nocodazole-induced cytotoxicity and compromised clonogenic potential, particularly in hematopoietic cell lines such as THP-1 (Wang et al., 2019; Rello-Varona et al., 2009).

Sequence analysis confirmed efficient CRISPR-mediated double-strand break induction, as reflected by the distribution of repair outcomes across all three independent experiments in the absence of nocodazole: the predominant outcome was the generation of insertions and deletions (InDels) via the non-homologous end-joining (NHEJ) pathway, whereas precise incorporation of the designed synonymous mutation occurred only rarely (mean= 1.33%; $p<0.0458$), and a smaller fraction of alleles remained wild type. These data demonstrate that the experimental conditions favored InDel formation far more frequently than successful introduction of the synonymous mutation, with only a minor proportion of unedited alleles persisting (**Figure 12b**). This is consistent with prior studies demonstrating the dominance of NHEJ in mammalian cells, particularly in hematopoietic lineages, and the challenge of biasing repair toward HDR (Brunet et al., 2019; Scully et al., 2019; Wienert et al., 2020). The prevalence of InDels reflects the fact that NHEJ operates throughout the cell cycle, whereas HDR is limited to the S/G2 phases. Importantly, in one clone it was possible to identify a monoallelic synonymous mutation (**Figure 12**). Sanger sequencing chromatograms demonstrated superimposed peaks corresponding to both the wild-type and edited nucleotides at the target site. In a true monoallelic edit, the relative signal intensities of wild-type and mutant bases are expected to be approximately equivalent. Although minor deviations in peak height are commonly observed due to intrinsic limitations of Sanger sequencing, the reverse-primer read in this instance displayed the characteristic pattern of a heterozygous modification. These findings provide proof of principle that homology-directed repair (HDR)–mediated precise editing can be achieved in THP-1 cells, albeit with low overall efficiency under the current experimental conditions.

To further validate editing outcomes at the sequence level, Sanger sequencing was also performed across the same target region for six DNMT3A knockout clones (KO1–KO6) using the forward primer (**Figure 13**). The wild-type THP-1 sequence served as a reference and revealed a clean electropherogram with no evidence of allelic disruption. In contrast, all six knockout clones exhibited overlapping peaks or signal degradation downstream of the expected Cas9 cut site, indicative of mixed allelic populations and heterogeneous InDel formation. Clones KO2 and KO4 in particular showed extensive sequence disruption with collapsed signal traces, consistent with biallelic editing and frameshift introduction. In KO1, KO3, KO5, and KO6, persistent background signal suggests a mixture of edited and possibly monoallelic sequences. These sequencing patterns confirm the diversity and complexity of repair outcomes associated with NHEJ and validate the editing status of each clone.

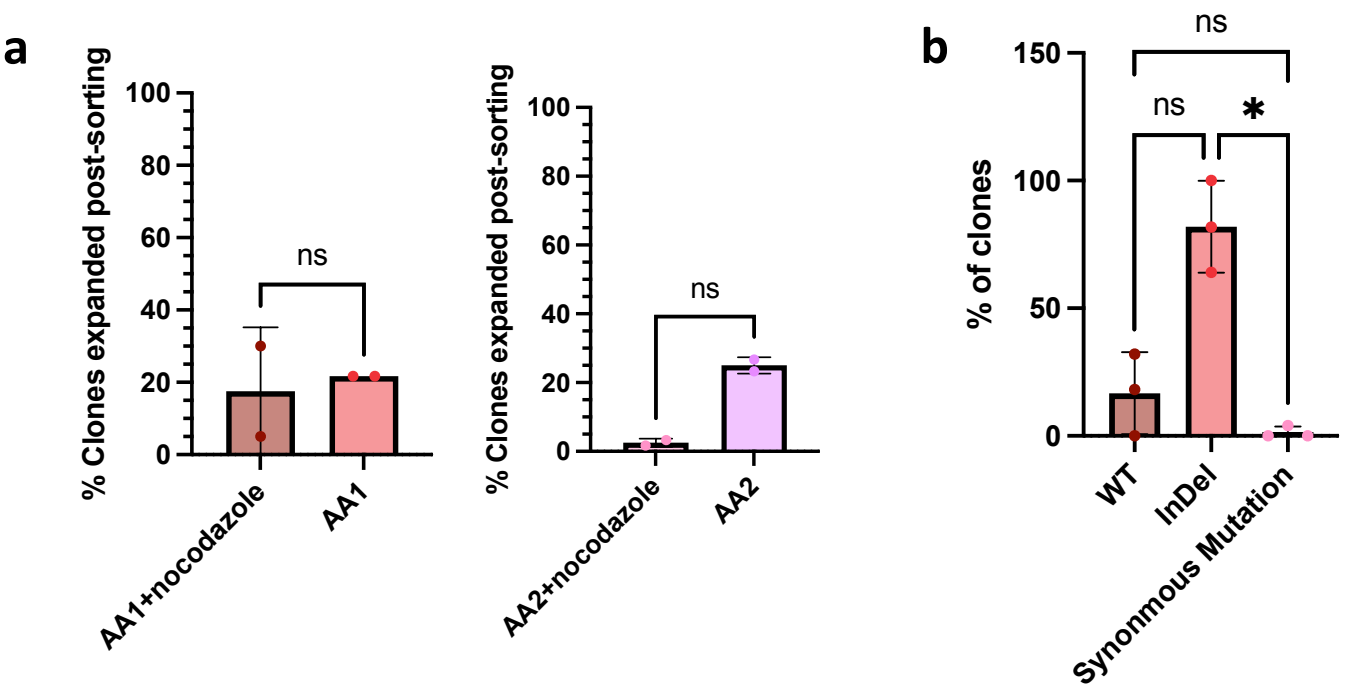

Figure 11. Single Cell Cloning Efficiency and CRISPR Editing Outcomes. a Single-Cell cloning efficiency of 60 clones with and without Nocodazole. Values are represented as mean ± SD of two individual experiments. Normalization was performed prior to analysis, and a non-parametric t-student test was performed, no significance due to lack of replicates. **b.** Distribution of CRISPR editing outcomes in clones. Normalization was performed prior to analysis, and a non-parametric one-way ANOVA was conducted using Kruskal-Wallis test also for multiple comparisons; *p<0.0458.

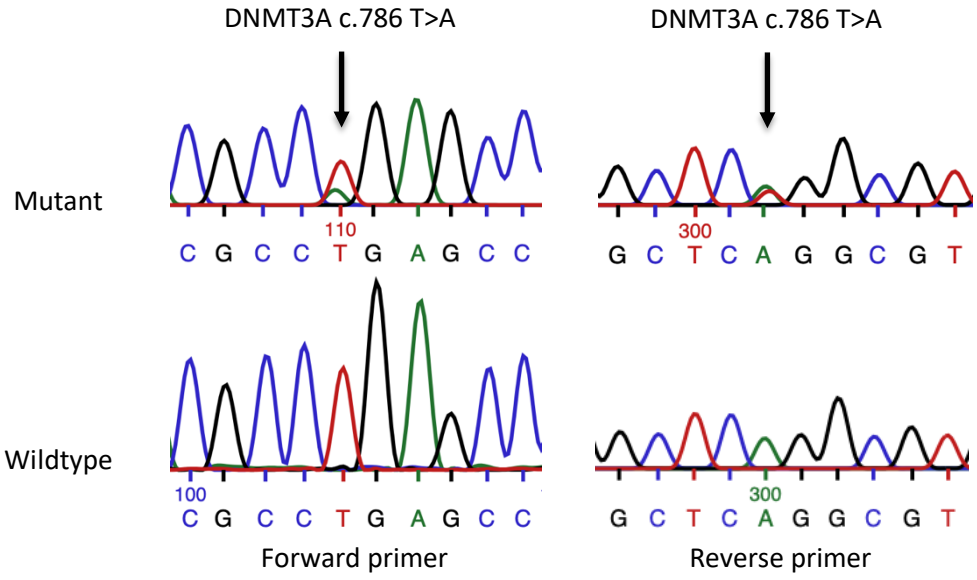

Figure 12. Representative WT and Mutant clone sequences showing CRISPR-induced mutation obtained by Sanger Sequencing with forward and reverse primers mentioned in Figure 7.

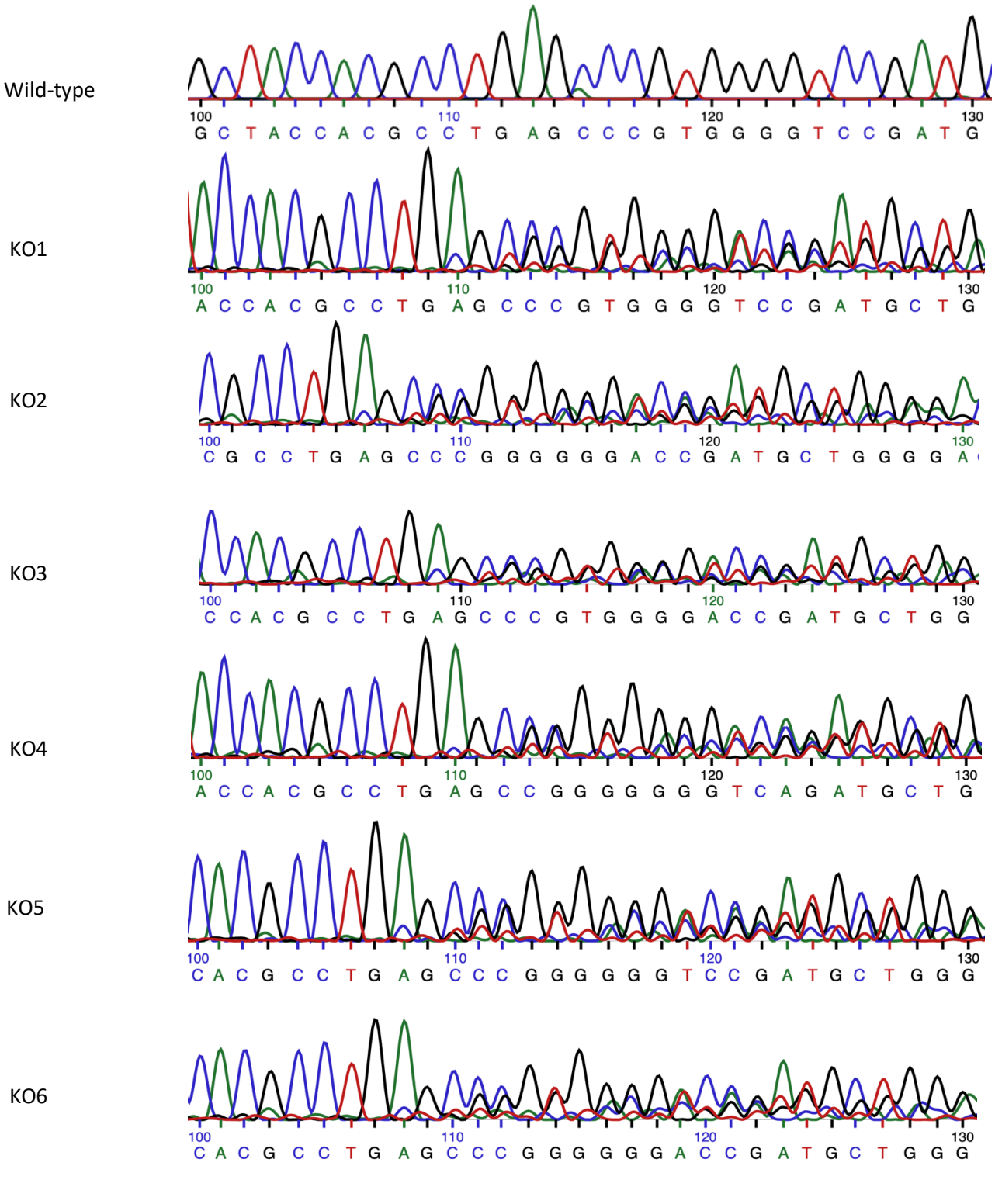

Figure 13. Sanger sequencing analysis of DNMT3A in wild-type and CRISPR-edited THP-1 clones. Representative chromatograms from forward strand Sanger sequencing are shown for THP-1 wild-type cells and six CRISPR-edited DNMT3A knockout clones (KO1–KO6).

4.4. Functional Assessment of DNMT3A Variants Through Overexpression in THP-1

To confirm robust overexpression of all DNMT3A constructs prior to transcriptional inhibition, transcript levels at the 0-hour timepoint were normalized to untransfected THP-1 wild-type cells using the ΔΔCt method (**Figure 14**). All constructs, including wildtype overexpressed, six synonymous variants (Syn1–Syn6), and the deletion variant (Del1), demonstrated elevated DNMT3A mRNA expression relative to endogenous levels in THP-1, with fold increases ranging from ~27-fold (Syn2) to over ~8,600-fold (Syn3). This confirms successful transgene expression across all constructs and validates that subsequent decay profiles reflect differences in transcript stability as well as some disparities in initial mRNA abundance.

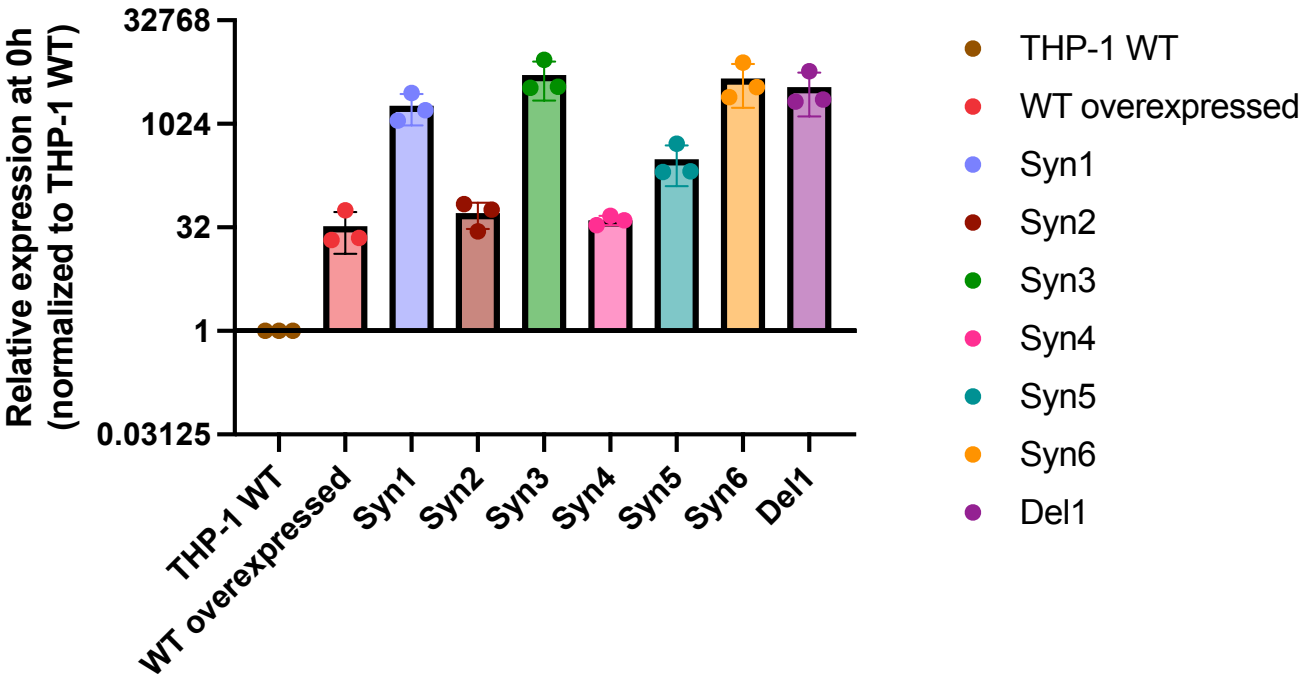

Figure 14. Relative expression of DNMT3A constructs at 0h normalized to untransfected THP-1 cells. Transcript levels were quantified by RT-qPCR at the 0-hour timepoint for wildtype overexpression (WT), six synonymous variants (Syn1–Syn6), and one deletion mutant (Del1), and were normalized to untransfected THP-1 wild-type cells using the ΔΔCt method. Data are presented as fold change (log_2 scale), mean ± SD of triplicates. Statistically significant differences in expression compared to THP-1 WT were assessed by Kruskal–Wallis test followed by Dunn's multiple comparisons test.

To investigate the impact of synonymous and deletion mutations on DNMT3A mRNA stability, a 24-hour time-course experiment was performed following transcriptional inhibition with actinomycin D. mRNA levels were quantified using RT-qPCR, and raw Ct values were measured for wildtype DNMT3A (WT)

overexpression, six synonymous variants (Syn1–Syn6), and one deletion variant (Del1), as shown in **Figure 15a**. The 0-hour time point represents untreated samples and serves as the baseline for transcript abundance. At this time point, Ct values ranged from 24.8 to 31.5 across constructs, with Syn3 showing the lowest Ct values (~24.8) and also Del1 (~25.7), indicating the highest initial level of DNMT3A mRNA, and Syn4 showing the highest (~31.5), indicating the lowest baseline expression. After actinomycin D treatment, all constructs exhibited increasing Ct values over time, consistent with progressive transcript degradation in the absence of new transcription. The WT construct showed moderate Ct increases over the 24-hour time course, from ~28 at 0 h to ~27.2 at 24 h, remaining within a relatively narrow range Syn1 showed a marked decrease in Ct values from 0 h (~29.9) to 30 minutes (~25.2), followed by a progressive increase, reaching ~30.7 at 2 hours. This profile indicates an early transcript stabilization or accumulation phase followed by accelerated decay, distinguishing it from the more gradual decline observed in WT. Syn2 displayed slightly lower Ct values than WT at early timepoints but remained within a comparable decay range. Syn3, by contrast, showed a sharp increase from ~24.8 at 0 h to ~38.4 by 24 h, indicating rapid transcript decay. Del1 also showed a steep increase, rising from ~25.7 at 0 h to ~27.6 at 2 h; however, the lower endpoint Ct values suggest potential plateauing or re-expression artefacts, warranting further clarification. Syn4, which began with the highest Ct values (~30.7 at 0 h), decreased dramatically at 30 min (~24.9) and then remained consistently elevated ~27.1 to ~30.2, between 1 and 24h, indicating both low baseline expression and rapid decay. Syn5 maintained intermediate Ct values throughout, increasing from ~28.3 at baseline to ~27.4 at 24 h. Syn6 began near WT levels (~27.3 at 0 h) and showed modest decay over time, ending at ~26.9 by 24 h, having its peak at 2h (~30.2). At the 2-hour timepoint, all synonymous and deletion constructs showed higher Ct values, and thus lower transcript abundance, compared to WT, with the exception of Syn2, which retained relatively lower Ct values.

To evaluate the reliability of RPL37A as a reference gene under these experimental conditions, its raw Ct values were measured in parallel across all constructs and timepoints (**Figure 15b**). RPL37A Ct values varied widely, ranging from 24.9 to 39.5, and displayed no consistent trend with time or construct, indicating unstable expression. For instance, Ct values for the same construct could fluctuate up or down between adjacent timepoints, independently of actinomycin D treatment duration. This variability disqualified RPL37A from being used for normalization. Consequently, all analyses of DNMT3A transcript decay were based solely on raw Ct values. These findings reveal distinct mRNA stability profiles among the DNMT3A constructs and demonstrate that both synonymous codon changes and sequence deletions can modulate transcript decay rates, with the deletion mutant showing the most pronounced destabilization.

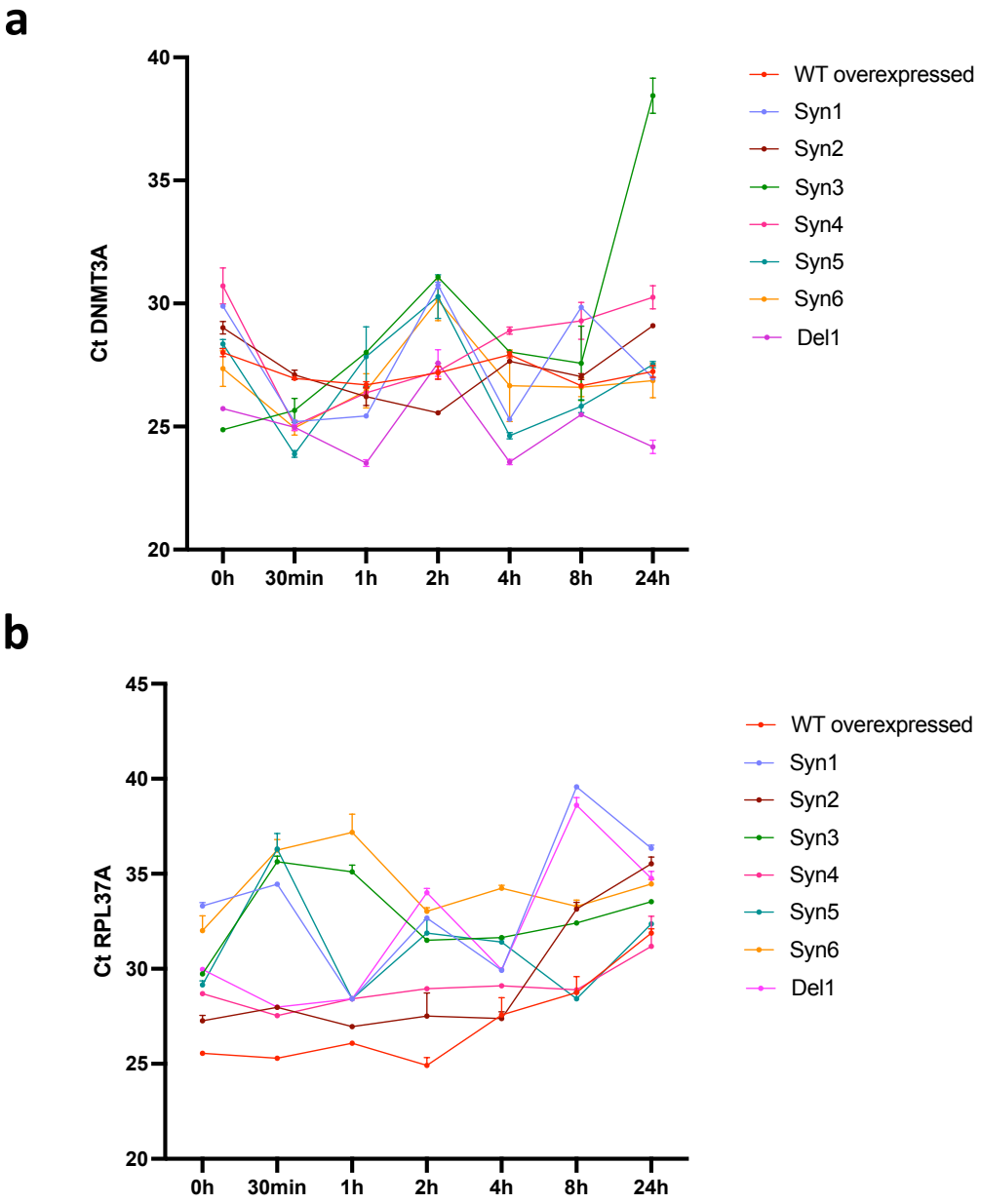

Figure 15. mRNA decay over 24 hours following transcriptional inhibition with actinomycin D. a. Raw Ct values from RT-qPCR were used to assess the mRNA stability of overexpressed wildtype DNMT3A (WT), six synonymous mutants (Syn1–Syn6), and one deletion mutant (Del1) across a 24-hour time course. Samples were collected at 0 h (untreated), 30 min, 1 h, 2 h, 4 h, 8 h, and 24 h post-treatment. Data represent mean ± SD of technical triplicates. Normalization was performed prior to statistical analysis. A non-parametric one-way ANOVA was conducted using Kruskal–Wallis test followed by Dunn's multiple comparisons. No statistically significant differences were found between any Syn and Del1 and WT overexpressed at any timepoint. **b.** Expression of RPL37A was measured across the same samples and timepoints to evaluate its suitability as a normalization control. Raw Ct values are shown as mean ± SD. Normalization and non-parametric statistical testing were conducted as described above. No significant differences were detected across most samples, except between: WT overexpressed and Syn1 ($p = 0.0082$), WT overexpressed and Syn3 ($p = 0.0137$), and WT overexpressed and Syn6 ($p = 0.0008$). These findings indicate instability in RPL37A expression under the tested conditions, precluding its use as a reliable reference gene.

To refine the analysis of early DNMT3A mRNA decay dynamics and enable higher temporal resolution of destabilization events, transcript abundance was quantified over a shortened 2-hour time course following transcriptional inhibition with actinomycin D (**Figure 16**). Constructs analyzed included wildtype DNMT3A overexpressed, six synonymous variants, and the deletion variant Del1. Transcript levels were normalized to the 0-hour timepoint, which corresponded to untreated cells and served as the baseline for relative quantification.

This focused time course was designed based on observations from the full 24-hour experiment (**Figure 15a**), which showed that most of the construct-specific divergence in decay kinetics occurred within the first 1 to 2 hours after transcriptional arrest. Beyond 2 hours, multiple samples, particularly the deletion mutant Del1 and the synonymous mutant Syn3, displayed rapid loss of signal, while others plateaued at high Ct values, limiting quantitative resolution and increasing measurement variability. The presence of saturation and floor effects at the 4-, 8-, and 24-hour timepoints limited the ability to resolve differences in mRNA stability across constructs. In particular, floor effects, where Ct values approached the detection limit of the assay due to near-complete transcript degradation, reduced the reliability of quantitative comparisons. These limitations justified the exclusion of later timepoints in favor of a focused 30min to 2 hour window, during which mRNA decay dynamics were most accurately and reproducibly observed.

Statistical comparisons were performed between each mutant and WT at each time point using Kruskal–Wallis tests followed by either Dunn's or Dunnett's post hoc adjustments. At the 1-hour timepoint, all except Syn1 showed significantly reduced transcript abundance relative to WT. No statistically significant differences were detected at 2 hours after correction for multiple comparisons. The complete statistical results are shown in the table beneath the plot in **Figure 16**.

These results confirm that the most discriminative phase for assessing transcript stability differences among DNMT3A constructs occurs within the first 2 hours following transcriptional arrest. Normalization to the 30 min enabled clear resolution of early decay kinetics, highlighting subtle but significant differences in mRNA stability attributable to both synonymous substitutions and deletion mutations.

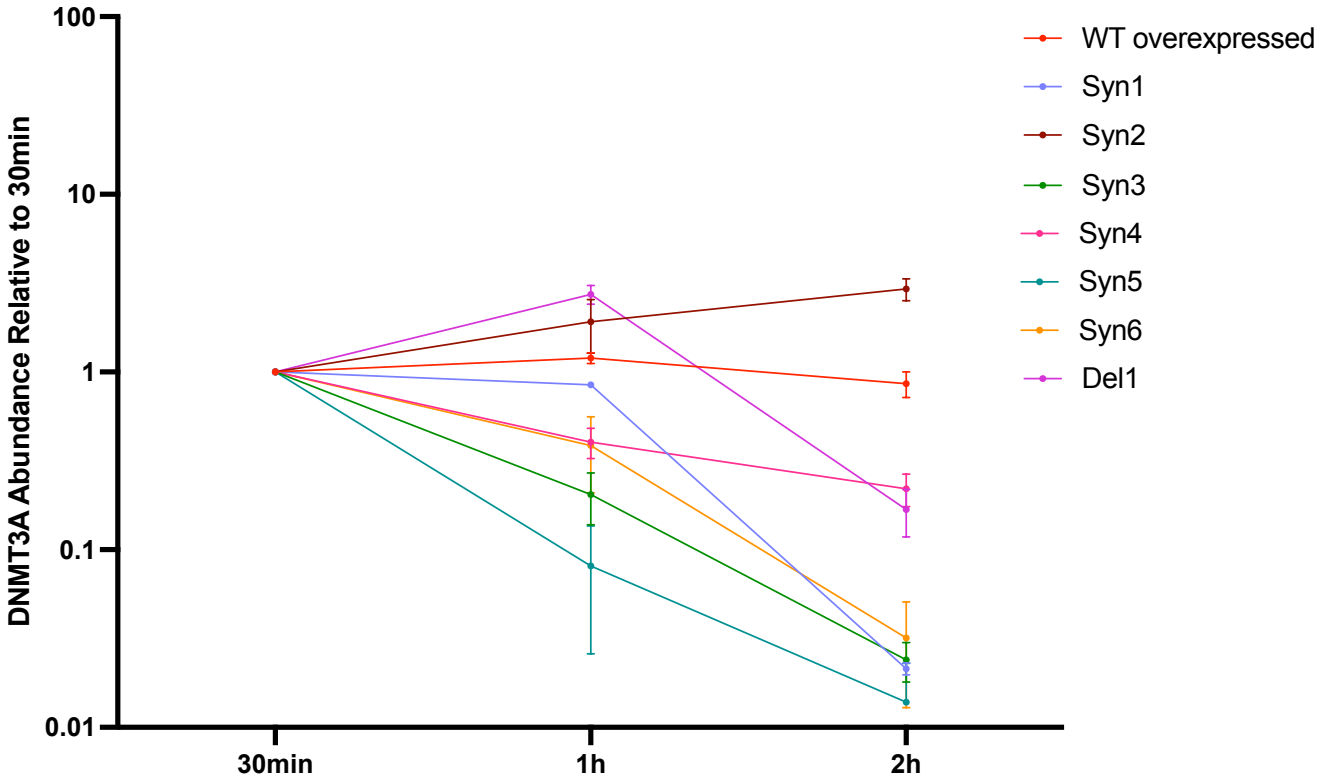

Statistical Comparison with WT overexpressed			
	Syn1	0.4609	>0,9999
	Syn2	0.0244	0.8332
	Syn3	0.0018	>0,9999
	Syn4	0.0118	>0,9999
	Syn5	0.0006	>0,9999
	Syn6	0.0099	>0,9999
	Del1	<0.0001	0.3475
		Kruskal-Wallis/Dunnett's	Kruskal-Wallis/Dunn's
Note: p adjusted <0.05 highlighted			

Figure 16. Short time-course analysis of DNMT3A mRNA decay normalized to 0 h. DNMT3A transcript abundance was measured over a 2-hour time course (0 h, 30 min, 1 h, 2 h) following actinomycin D treatment in wildtype overexpressed DNMT3A, Syn1, Syn2, Syn3, Syn4, Syn5, Syn6, and Del1. Data are shown as mean ± SD, normalized to the 0-hour timepoint. A non-parametric one-way ANOVA with Kruskal–Wallis test and Dunn's or Dunnett's multiple comparison correction was performed. Statistically significant reductions in transcript levels relative to WT are observed in the table above.

5. Discussion

This study set out to functionally interrogate synonymous DNMT3A mutations within a hematopoietic context by combining CRISPR/Cas9 genome engineering in THP-1 monocytic cells with overexpression assays. Synonymous mutations, once assumed to be biologically silent, are now recognized as modulators of gene expression through their potential effects on mRNA stability, splicing, and translation kinetics (Shen et al., 2022; Zupek et al., 2014). These findings reinforce this paradigm, demonstrating that specific synonymous DNMT3A variants can drive substantial changes in transcript abundance and decay kinetics. In the setting of clonal hematopoiesis, even subtle changes in DNMT3A amount can confer a selective advantage that facilitates long-term clonal expansion and contributes to disease risk (Jaiswal et al., 2017; Venugopal et al., 2021; Yu et al., 2023).

Efficient genome editing in suspension hematopoietic cell lines remains technically challenging (Lino et al., 2018; Kim et al., 2014). Systematic optimization of nucleofection protocols identified FF100 as optimal for balancing transfection efficiency and cell viability, which is in line with other studies in myeloid models (**Figure 6d**) (Lino et al., 2018). Notably, FF100 is not only supported by the experimental data presented in this study but is also the program recommended by Lonza for THP-1 monocytic cells, based on extensive internal benchmarking in hematopoietic suspension models. By contrast, alternative programs such as DK100 and CM138 resulted in significantly poorer outcomes, either by reducing transfection efficiency or inducing marked cytotoxicity. These observations agree with prior reports showing that harsh nucleofection settings, while sometimes enhancing delivery in adherent lines, can cause irreversible membrane damage and trigger apoptosis in fragile suspension cultures such as THP-1 or $CD34^+$ progenitors (Komor et al., 2016). It is well documented that myeloid cells exhibit heightened sensitivity to electroporation-induced stress, leading to transient mitochondrial dysfunction and activation of stress-response pathways that can sharply reduce post-nucleofection survival (Kim et al., 2014), consistent with our findings.

In addition, the use of FITC-labeled donor oligonucleotides, while helpful for monitoring delivery, resulted in reduced post-nucleofection viability. This effect is consistent with prior evidence that covalent attachment of bulky fluorophores such as FITC can compromise oligonucleotide stability and increase recognition by innate immune sensors, leading to interferon-mediated cytotoxicity in sensitive cells (Delehedde et al., 2021). Similar observations were reported in primary hematopoietic cells, where fluorophore-modified donors triggered elevated cell death without significantly impacting homology-directed repair efficiency (Li et al., 2020). Collectively, these data highlight that while fluorescent labeling can be a useful tracking tool, it carries biological costs in fragile hematopoietic cell lines that must be carefully weighed when designing genome-editing experiments.

Despite employing nocodazole-mediated G2/M synchronization to bias repair toward homology-directed repair (HDR), most editing outcomes were dominated by non-homologous end joining (NHEJ), consistent with reports that hematopoietic progenitors exhibit an intrinsic preference for NHEJ, coupled with considerable fitness costs under prolonged synchronization (Scully et al., 2019; Wienert et al., 2020). As observed in **Figure 11a**, cell survival post-nocodazole was reduced to 1–3 %, compared to 21–27 % in unsynchronized controls, highlighting the technical bottleneck of HDR-based editing in these systems. Nevertheless, one monoallelic clone with a patient-derived synonymous mutation was successfully achieved, as well as 6 possibly monoallelic knockouts, demonstrating that precise integration is possible, albeit at low frequency (**Figure 12 and Figure 13**). These data support the growing consensus that emerging tools such as base editors and prime editors, which circumvent double-strand breaks and HDR, are likely to be more effective for introducing precise point mutations in hematopoietic models (Anzalone et al., 2020).

Western blot analysis (**Figure 9a**) was first performed to evaluate DNMT3A protein expression across the six CRISPR-engineered clones. This step was essential because genomic editing outcomes detected at the DNA level do not always correlate with protein loss or altered protein integrity. Therefore, a direct assessment of protein expression provides critical functional validation. In this assay, HEK293T wild-type and DNMT3A-overexpressing cells were included as positive controls, as these are well-characterized epithelial cells known to express DNMT3A at robust and consistent levels (Zhang et al., 2025), and their banding pattern allows the confirmation of antibody specificity. Additionally, $CD34^+$ primary hematopoietic cells were included as a physiologically relevant control representing a non-leukemic hematopoietic population, enabling direct comparison to THP-1 backgrounds. As expected, the DNMT3A band in HEK cells migrated slightly higher than in THP-1 (~150 kDa vs. ~118–125 kDa). This is consistent with prior reports indicating cell-type–specific post-translational modifications, particularly differential phosphorylation and glycosylation patterns, which can alter electrophoretic mobility without changing the underlying coding sequence (Zhang et al., 2008). Of note, the α-tubulin loading control band appeared slightly fainter in THP-1 wild-type sample compared to the other samples. This difference may reflect cell-type–specific variations in basal cytoskeletal protein abundance and altered microtubule turnover in leukemic monocytic cells, which often display reduced steady-state tubulin content compared to adherent cells (Sallee et al., 2021). Analysis of the WES data revealed that only KO2 and KO4 lacked detectable DNMT3A protein bands between ~118 and 130 kDa, strongly suggesting protein-level knockout in these two clones. In contrast, KO1, KO3, KO5, and KO6 retained visible DNMT3A bands despite targeted editing, indicating that these alleles likely resulted in in-frame indels or generated truncated proteins still detectable by the antibody. Importantly, it remains undetermined whether these CRISPR-induced mutations occurred in homozygous or heterozygous configurations, as allele phasing information is lacking. Without evidence of biallelic disruption, residual protein expression in KO1, KO3, KO5, and KO6 may reflect partial editing or the presence of unmodified alleles. Moreover, considering

that CRISPR editing often generates small insertions or deletions, the distinction between in-frame and out-of-frame indels becomes critical. A 5-nucleotide indel, for example, would disrupt the reading frame and likely introduce a premature termination codon, potentially triggering nonsense-mediated decay (Deneault, 2024). Conversely, in-frame deletions may preserve the reading frame and result in internally truncated proteins that retain immunoreactivity, consistent with the DNMT3A signal observed in these four clones.

This observation is further supported by the normalized expression values (**Figure 9b**) which show that these clones exhibit DNMT3A protein levels comparable to the THP-1 wild-type control. Therefore, these clones likely do not represent knockouts at the protein level. In contrast, THP-1 cells, representing a more differentiated monocytic lineage, typically show reduced DNMT3A expression, particularly during terminal differentiation (Huang et al., 2016). Although the two samples were lysed using different buffers, Cell Lytic M for $CD34^+$ cells and HEK293T, and SDS-containing buffer for THP-1 cells, control experiments showed that THP-1 lysed with Cell Lytic M yielded no detectable DNMT3A band. This suggests that the observed difference in DNMT3A signal intensity reflects a genuine biological disparity in protein abundance, rather than differences in extraction efficiency. To accurately compare DNMT3A protein expression between cell types, consistent lysis conditions, preferably using a strong denaturing buffer like SDS, are essential. This highlights the critical importance of performing Western blot verification, as genomic alterations alone (e.g., frameshift predictions) may not capture translational rescue mechanisms or the generation of truncated but still immunoreactive proteins (Kim et al., 2020).

To complement the normalized protein quantification, DNMT activity assays were performed across the same THP-1 knockout clones (**Figure 10**). When comparing the Western blot–based quantification (normalized WES signal) to the functional activity readouts, several points emerge regarding assay sensitivity. The WES platform, while highly sensitive in detecting residual protein levels after normalization to loading controls, primarily reflects total immunoreactive protein and does not distinguish between catalytically competent and impaired forms. In contrast, the DNMT activity assay directly measures enzymatic function and is therefore more sensitive to functional impairments that may not alter antibody recognition. For instance, KO3 and KO5 display normalized WES signals comparable to wild type, indicating preserved DNMT3A protein levels, yet both show substantial reductions in DNMT activity. This discrepancy suggests the presence of structurally altered but immunoreactive proteins, potentially harboring in-frame deletions affecting the methyltransferase catalytic core or cofactor-binding motifs, as described in mechanistic studies of DNMT3A (Kunert, 2024). Conversely, KO2 demonstrates reduced normalized WES signal and a concomitant loss of activity, indicative of a non-functional protein product with partial degradation, while KO4 exhibits both absent WES signal and complete absence of activity, representing a true protein and functional knockout. These distinctions underscore the complementary nature of the two techniques:

normalized WES allows sensitive detection of residual or truncated protein, while activity assays provide a more functionally stringent assessment. Integrating both datasets is critical, as residual non-functional proteins can exert dominant-negative effects or interfere with multiprotein complexes, potentially leading to phenotypes divergent from those of complete null alleles.

As shown in **Table 11**, DNMT3A knockout clones exhibited variable proliferation rates relative to THP-1 wildtype cells. The wildtype line displayed a doubling time of approximately 48 hours, consistent with the reference value reported by DSMZ. Clones KO2, KO3, and KO5 demonstrated shorter doubling times, suggestive of enhanced proliferative capacity, whereas KO1, KO4, and KO6 exhibited longer doubling times, indicating relative growth delay. Despite these differences, no statistically significant variations were observed between the knockout clones and the wildtype across three independent biological replicates. These findings imply that DNMT3A disruption does not impart a uniform effect on cell cycle progression but instead leads to clone-specific alterations in proliferation. From a biological perspective, DNMT3A loss has been associated with epigenetic reprogramming and altered transcriptional control in hematopoietic stem cells, potentially influencing proliferative behavior through changes in DNA methylation and chromatin accessibility (Challen et al., 2012; Jaiswal et al., 2017). Therefore, even partial reductions in DNMT3A expression, as observed in some clones, could reshape epigenetic landscapes and transcriptional networks, leading to divergent growth kinetics. In line with this, cell viability monitoring over a 15-day period (**Figure 8c**) revealed high overall survival across all clones, including WT, though transient fluctuations were noted. All cell lines showed a sharp but temporary drop in viability around day 2, followed by recovery. KO5 and KO6 exhibited an additional decline around day 6, while KO2 showed a viability decrease at day 10. Despite these episodic dips, all clones ultimately returned to baseline viability, and no statistically significant differences in overall cell survival were found when compared to the wildtype. These transient effects may reflect early adaptation to clonal outgrowth or stress responses linked to DNMT3A disruption, further supporting a model of functional heterogeneity among the knockout clones.

The present study reveals that both synonymous and deletion mutations within the DNMT3A coding sequence significantly modulate mRNA stability, with distinct temporal decay profiles evident from both long (24 h) and short (2 h) transcriptional inhibition time courses. These findings underscore the critical role of local coding sequence features in determining post-transcriptional transcript fate and align with growing evidence that mRNA stability is not merely a passive consequence of sequence content but an actively regulated property with functional consequences for gene expression output. Importantly, all wildtype overexpressed, synonymous variants, and the deletion mutant, were robustly overexpressed at baseline relative to endogenous DNMT3A levels in THP-1 cells, as confirmed by ΔΔCt-based quantification. Therefore, the observed differences in mRNA decay between constructs are unlikely to reflect variability in initial

transcript abundance and instead point to genuine stability effects associated with specific sequence changes (**Figure 14**).

From the 24-hour RT-qPCR time course (**Figure 15a**), it was apparent that several synonymous mutants, exhibited more rapid mRNA decay relative to the wildtype (WT) construct, as reflected by faster increases in raw Ct values. In contrast, Syn2 and Syn4 displayed similar decay trajectories to WT, suggesting that not all synonymous codon substitutions perturb mRNA stability to the same extent. These long-range decay kinetics established that the coding sequence of DNMT3A contains both codon-dependent and region-specific determinants of transcript longevity. To resolve early-phase decay events that may be obscured by transcript depletion or saturation effects at later timepoints, we implemented a higher-resolution 30min to 2 h analysis using transcript levels normalized to the 30 min condition (**Figure 16**). The short time course corroborated and extended the findings of the full decay profile. Syn3, which trended toward instability in the long-time course without reaching statistical significance at individual timepoints, showed a striking and continuous drop in relative abundance during the first 2 hours, identifying it as a likely unstable variant. All Syn 2-6 and Del1, revealed statistically significant reductions in abundance at the 1 h mark, supporting the conclusion that their destabilization occurs acutely and may be partially masked over longer intervals. Conversely, Syn1, did not show significant differences at early timepoints, suggesting that their destabilization may involve cumulative or delayed mechanisms. These observations highlight the complementarity of short- and long-term transcript decay analyses for capturing both acute and sustained regulatory effects.

These results contribute to a growing body of literature showing that synonymous codon changes, traditionally considered silent, can profoundly impact mRNA fate. Codon usage has been shown to affect transcript stability via codon optimality, where rare codons can slow ribosome transit and expose mRNA to decay machinery (Presnyak et al., 2015; Narula et al., 2023). More recently, Supek et al. (2021) demonstrated that synonymous mutations frequently act as driver mutations in cancer by altering RNA stability and translation efficiency, further reinforcing the functional importance of codon identity. In the context of DNMT3A, a gene frequently mutated in hematologic malignancies and essential for epigenetic regulation, such codon-level control may represent an additional layer of post-transcriptional regulation with phenotypic consequences.

The pronounced instability observed in Del1 further implicates cis-acting elements within the deleted region as critical for transcript maintenance. This may include binding sites for RNA-stabilizing proteins, secondary structures that prevent exonucleolytic degradation, or sequence motifs such as AU-rich elements (AREs) known to regulate mRNA half-life (Mayr, 2017; Bazzini et al., 2020). The nearly complete loss of Del1 transcript by 24 h, along with its consistently lower abundance across early timepoints, suggests that removal

of these elements can override codon-related effects and drive rapid degradation through general mRNA decay pathways.

The failure of RPL37A to serve as a stable reference gene in these experiments further emphasizes the importance of validating normalization controls under each specific experimental context. Prior studies have demonstrated that housekeeping genes, including ribosomal proteins, can display variable expression under transcriptional inhibition or cellular stress (Vandesompele et al., 2021; de Jonge et al., 2007), and our findings are consistent with these observations. The decision to analyze only raw Ct values, while limiting in terms of relative quantification, ensured that observed differences reflect genuine transcript-specific decay dynamics rather than artifacts of normalization.

Together, these data indicate that both synonymous codon usage and non-coding sequence context within DNMT3A significantly affect transcript stability, operating through distinct temporal kinetics. Early destabilization, as observed for Syn1, Syn3, and Syn5, likely reflects immediate susceptibility to decay machinery, whereas late-phase degradation seen in Syn2 and Syn4 may reflect more gradual loss of protection or translational disengagement. Deletion of structural elements, as in Del1, results in robust, sustained destabilization, emphasizing the combinatorial nature of mRNA stability regulation.

Future studies will be required to define the precise mechanisms underlying these effects, including ribosome profiling to assess translational efficiency, SHAPE-MaP or related technologies to examine secondary structure, and crosslinking immunoprecipitation (CLIP) assays to identify RNA-binding proteins interacting with affected regions. Importantly, the demonstrated effects of synonymous and deletion mutations on mRNA stability support a model in which coding sequence variation directly contributes to post-transcriptional regulation, with potential implications for DNMT3A function in health and disease. To further resolve the allelic complexity and confirm the precise sequence architecture of CRISPR-edited clones, future work should also include subcloning of allele-specific PCR products followed by Sanger sequencing. This approach allows unambiguous phasing of individual alleles, which is essential for distinguishing compound heterozygosity, assessing editing outcomes on each chromosome independently, and identifying potential mosaicism or unintended editing events that may not be detectable in bulk sequencing traces.

These results hold significant implications for the understanding of clonal hematopoiesis and the pathogenesis of DNMT3A-mutant hematologic disorders. While clonal hematopoiesis of indeterminate potential (CHIP) is most frequently driven by missense or truncating mutations in DNMT3A, the present data demonstrate that synonymous variants are also capable of altering transcript abundance and stability, thereby contributing to functional heterogeneity. Even modest but sustained changes in DNMT3A expression over time have the potential to reshape DNA methylation landscapes, perturb hematopoietic stem cell

self-renewal and differentiation programs, and ultimately promote clonal selection and expansion within the hematopoietic compartment (Venugopal et al., 2021; Jaiswal et al., 2017; Yu et al., 2023). The transcriptional dysregulation identified in this study provides a compelling mechanistic link between ostensibly silent coding variation and altered cellular phenotypes, thereby expanding the recognized mutational spectrum that can influence clonal fitness and predisposition to malignant transformation.

Several limitations of this study must be acknowledged. First, the low efficiency of homology-directed repair (HDR), combined with the cytotoxicity associated with nocodazole-mediated G2/M synchronization, slowed down and restricted our ability to generate multiple precise knock-in clones for functional replication. HDR inefficiency in hematopoietic suspension cells is well documented, reflecting intrinsic preferences for non-homologous end joining and cell-cycle heterogeneity (Wienert et al., 2020; Scully et al., 2019). Second, the transient overexpression assays employed in this work may not fully recapitulate endogenous regulatory dynamics, including transcriptional feedback loops and chromatin context. Moreover, mRNA measurements alone do not always correspond to protein abundance or enzymatic activity, underscoring the need for complementary proteomic and functional assays. Third, previous transcriptomic profiles confirm that RPL37A is expressed at significantly higher levels in THP-1 cells than DNMT3A. Because qPCR normalization assumes stable and proportionate reference gene expression, using a highly abundant transcript like RPL37A can compress the apparent dynamic range of low-abundance targets, potentially masking subtle yet biologically meaningful fluctuations in DNMT3A mRNA. In addition, we observed variability in RPL37A Ct values under constructs, suggesting that its transcription may itself be perturbed under extreme overexpression conditions. Future studies should therefore include multiple housekeeping genes of comparable abundance and implement transcriptome-wide normalization strategies to minimize these artifacts. Finally, as THP-1 cells are derived from an acute monocytic leukemia, their epigenetic and transcriptional landscapes does not accurately reflect primary hematopoietic stem and progenitor cells (HSPCs). Validation in primary hematopoietic models or *in vivo* systems will be essential to establish the physiological relevance of these findings.

Future work should focus on integrating precise genome-editing strategies that overcome the limitations of HDR. Base editors and prime editors, which directly install point mutations without double-strand breaks, offer a promising avenue for modeling synonymous variants with higher fidelity (Anzalone et al., 2020). In parallel, high-throughput saturation mutagenesis in a permissive model such as HCT116 cells, a colorectal carcinoma line that exhibits exceptional HDR efficiencies, stable clonal expansion, and a well-characterized genetic background (Funk et al., 2025), would enable systematic interrogation of thousands of synonymous positions at scale. HCT116 cells are particularly suited because they tolerate extensive editing with minimal cell-cycle disruption, allowing for the robust recovery of edited clones for downstream multi-omics profiling.

These large-scale screens should then be complemented by focused validation in primary HSPCs or xenotransplantation models to assess hematopoietic relevance directly.

At the mechanistic level, future investigations should integrate multi-omics approaches to link nucleotide-level changes to cellular phenotypes. Combining transcriptomics, ribosome profiling, and quantitative proteomics with genome-wide methylation analysis will allow a comprehensive assessment of how synonymous variants influence not only mRNA turnover but also translational efficiency and downstream epigenetic states (Brunet et al., 2019). High-resolution RNA structure probing (e.g., SHAPE-MaP) and RNA-protein interaction mapping (e.g., CLIP-seq) will further elucidate how individual substitutions remodel binding landscapes of regulatory proteins or expose/destabilize structural motifs (Hanson & Coller, 2017). Finally, whole-genome sequencing should be implemented to monitor potential off-target editing events, ensuring specificity as genome-engineering technologies are advanced toward clinical translation.

The findings presented here highlight that synonymous DNMT3A variants, long assumed to be functionally neutral, can exert significant effects on transcript stability and abundance. In the context of clonal hematopoiesis, these subtle alterations in DNMT3A amount may recalibrate DNA methylation programs, skew hematopoietic stem cell fate decisions, and provide a competitive advantage that promotes clonal outgrowth (Venugopal et al., 2021; Yu et al., 2023). Clinically, this suggests that patients carrying synonymous DNMT3A mutations might harbor previously unrecognized risks for hematologic progression or cardiovascular morbidity, expanding the spectrum of variants warranting surveillance in CHIP (Jaiswal et al., 2017). Moreover, these data support the inclusion of synonymous changes in diagnostic pipelines and variant-interpretation frameworks, which historically prioritized only nonsynonymous alterations.

In conclusion, this study demonstrates that synonymous DNMT3A mutations are not transcriptionally silent. Rather, they can induce profound and construct-specific effects on mRNA abundance and stability, with potential to reshape epigenetic landscapes and influence clonal fitness. By combining functional genomics with rigorous transcriptomic analysis, this work expands the mutational spectrum relevant to clonal hematopoiesis and assesses the need to reassess how synonymous variation is interpreted in both research and clinical contexts. Future integration of precise genome-editing tools, saturation mutagenesis in high-HDR systems such as HCT116, and multi-layered molecular profiling will be instrumental in defining the full regulatory impact of these subtle genetic alterations. Collectively, these approaches will deepen our understanding of how small coding changes reverberate through gene regulation networks, ultimately informing risk stratification and therapeutic strategies in hematologic disease.

6. References

Akiyama, T., & Yamamoto, T. (2021). Regulation of Early Lymphocyte Development via mRNA Decay Catalyzed by the CCR4-NOT Complex. *Frontiers in Immunology*, *12*. https://doi.org/10.3389/fimmu.2021.715675

Anzalone, A. V., Koblan, L. W., & Liu, D. R. (2020). Genome editing with CRISPR–Cas nucleases, base editors, transposases and prime editors. *Nature Biotechnology*, *38*(7), 824–844. https://doi.org/10.1038/s41587-020-0561-9

Basheer, F., & Vassiliou, G. (2021). Mouse Models of Myeloid Malignancies. *Cold Spring Harbor Perspectives in Medicine*, *11*(1), a035535. https://doi.org/10.1101/cshperspect.a035535

Belyavsky, A., Petinati, N., & Drize, N. (2021). Hematopoiesis during Ontogenesis, Adult Life, and Aging. *International Journal of Molecular Sciences*, *22*(17), Article 17. https://doi.org/10.3390/ijms22179231

Bhat, A. A., Nisar, S., Singh, M., Ashraf, B., Masoodi, T., Prasad, C. P., Sharma, A., Maacha, S., Karedath, T., Hashem, S., Yasin, S. B., Bagga, P., Reddy, R., Frennaux, M. P., Uddin, S., Dhawan, P., Haris, M., & Macha, M. A. (2022). Cytokine- and chemokine-induced inflammatory colorectal tumor microenvironment: Emerging avenue for targeted therapy. *Cancer Communications*, *42*(8), 689–715. https://doi.org/10.1002/cac2.12295

Brown, G. (2022). Hematopoietic and Chronic Myeloid Leukemia Stem Cells: Multi-Stability versus Lineage Restriction. *International Journal of Molecular Sciences*, *23*(21), Article 21. https://doi.org/10.3390/ijms232113570

Brule, C. E., & Grayhack, E. J. (2017). Synonymous Codons: Choose Wisely for Expression. *Trends in Genetics*, *33*(4), 283–297. https://doi.org/10.1016/j.tig.2017.02.001

Brunet, E., & Jasin, M. (2018). Induction of Chromosomal Translocations with CRISPR-Cas9 and Other Nucleases: Understanding the Repair Mechanisms That Give Rise to Translocations. In Y. Zhang (Ed.), *Chromosome Translocation* (pp. 15–25). Springer. https://doi.org/10.1007/978-981-13-0593-1_2

Buscarlet, M., Provost, S., Zada, Y. F., Barhdadi, A., Bourgoin, V., Lépine, G., Mollica, L., Szuber, N., Dubé, M.-P., & Busque, L. (2017). DNMT3A and TET2 dominate clonal hematopoiesis and demonstrate benign phenotypes and different genetic predispositions. *Blood*, *130*(6), 753–762. https://doi.org/10.1182/blood-2017-04-777029

Cai, Z., Kotzin, J. J., Ramdas, B., Chen, S., Nelanuthala, S., Palam, L. R., Pandey, R., Mali, R. S., Liu, Y., Kelley, M. R., Sandusky, G., Mohseni, M., Williams, A., Henao-Mejia, J., & Kapur, R. (2018). Inhibition of Inflammatory

Signaling in Tet2 Mutant Preleukemic Cells Mitigates Stress-Induced Abnormalities and Clonal Hematopoiesis. *Cell Stem Cell*, *23*(6), 833-849.e5. https://doi.org/10.1016/j.stem.2018.10.013

Caiado, F., & Manz, M. G. (2025). Clonal Hematopoiesis: Impact on Health and Disease. *Hematological Oncology*, *43*(S2), e70075. https://doi.org/10.1002/hon.70075

Cao, X., Zhang, L., Wang, X., Chen, Z., Zheng, C., Chen, L., Zhou, H., Cai, J., Hu, Z., Tian, Y., Gu, R., Huang, Y., & Wang, Z. (2023). Cardiovascular disease and all-cause mortality associated with individual and combined cardiometabolic risk factors. *BMC Public Health*, *23*(1), 1725. https://doi.org/10.1186/s12889-023-16659-8

Ceccaldi, R., Rondinelli, B., & D'Andrea, A. D. (2016). Repair Pathway Choices and Consequences at the Double-Strand Break. *Trends in Cell Biology*, *26*(1), 52–64. https://doi.org/10.1016/j.tcb.2015.07.009

Challen, G. A., Sun, D., Jeong, M., Luo, M., Jelinek, J., Berg, J. S., Bock, C., Vasanthakumar, A., Gu, H., Xi, Y., Liang, S., Lu, Y., Darlington, G. J., Meissner, A., Issa, J.-P. J., Godley, L. A., Li, W., & Goodell, M. A. (2012). Dnmt3a is essential for hematopoietic stem cell differentiation. *Nature Genetics*, *44*(1), 23–31. https://doi.org/10.1038/ng.1009

Chen, J. S., Dagdas, Y. S., Kleinstiver, B. P., Welch, M. M., Sousa, A. A., Harrington, L. B., Sternberg, S. H., Joung, J. K., Yildiz, A., & Doudna, J. A. (2017). Enhanced proofreading governs CRISPR–Cas9 targeting accuracy. *Nature*, *550*(7676), 407–410. https://doi.org/10.1038/nature24268

Chen, L., Pronk, E., van Dijk, C., Bian, Y., Feyen, J., van Tienhoven, T., Yildirim, M., Pisterzi, P., de Jong, M. M. E., Bastidas, A., Hoogenboezem, R. M., Wevers, C., Bindels, E. M., Löwenberg, B., Cupedo, T., Sanders, M. A., & Raaijmakers, M. H. G. P. (2023). A Single-Cell Taxonomy Predicts Inflammatory Niche Remodeling to Drive Tissue Failure and Outcome in Human AML. *Blood Cancer Discovery*, *4*(5), 394–417. https://doi.org/10.1158/2643-3230.BCD-23-0043

Delehedde, C., Even, L., Midoux, P., Pichon, C., & Perche, F. (2021). Intracellular Routing and Recognition of Lipid-Based mRNA Nanoparticles. *Pharmaceutics*, *13*(7), Article 7. https://doi.org/10.3390/pharmaceutics13070945

Deneault, E. (2024). Recent Therapeutic Gene Editing Applications to Genetic Disorders. *Current Issues in Molecular Biology*, *46*(5), Article 5. https://doi.org/10.3390/cimb46050255

Díaz Navarro, A. (2022). *Development of a tool for the identification of somatic mutations and analysis of non-coding mutations in cancer* [Doctoral thesis]. https://digibuo.uniovi.es/dspace/handle/10651/65757

Doehner, W., Böhm, M., Boriani, G., Christersson, C., Coats, A. J. S., Haeusler, K. G., Jones, I. D., Lip, G. Y. H., Metra, M., Ntaios, G., Savarese, G., Shantsila, E., Vilahur, G., & Rosano, G. (2023). Interaction of heart failure and

stroke: A clinical consensus statement of the ESC Council on Stroke, the Heart Failure Association (HFA) and the ESC Working Group on Thrombosis. *European Journal of Heart Failure*, *25*(12), 2107–2129. https://doi.org/10.1002/ejhf.3071

Doench, J. G., Fusi, N., Sullender, M., Hegde, M., Vaimberg, E. W., Donovan, K. F., Smith, I., Tothova, Z., Wilen, C., Orchard, R., Virgin, H. W., Listgarten, J., & Root, D. E. (2016). Optimized sgRNA design to maximize activity and minimize off-target effects of CRISPR-Cas9. *Nature Biotechnology*, *34*(2), 184–191. https://doi.org/10.1038/nbt.3437

Dorsheimer, L., Assmus, B., Rasper, T., Ortmann, C. A., Abou-El-Ardat, K., Kiefer, K. C., Hoffmann, J., Seeger, F., Bonig, H., Dimmeler, S., Zeiher, A. M., & Rieger, M. A. (2020). Hematopoietic alterations in chronic heart failure patients by somatic mutations leading to clonal hematopoiesis. *Haematologica*, *105*(7), e328–e332. https://doi.org/10.3324/haematol.2019.224402

Doudna, J. A., & Charpentier, E. (2014). The new frontier of genome engineering with CRISPR-Cas9. *Science*, *346*(6213), 1258096. https://doi.org/10.1126/science.1258096

Eaves, C. J. (2015). Hematopoietic stem cells: Concepts, definitions, and the new reality. *Blood*, *125*(17), 2605–2613. https://doi.org/10.1182/blood-2014-12-570200

Fabre, M. A., & Vassiliou, G. S. (2025). Clonal haematopoiesis. In *Hoffbrand's Postgraduate Haematology* (pp. 745–756). John Wiley & Sons, Ltd. https://doi.org/10.1002/9781119706687.ch38

Fackenthal, J. D. (2023). Alternative mRNA Splicing and Promising Therapies in Cancer. *Biomolecules*, *13*(3), Article 3. https://doi.org/10.3390/biom13030561

Ferreira, H. J., Heyn, H., Vizoso, M., Moutinho, C., Vidal, E., Gomez, A., Martínez-Cardús, A., Simó-Riudalbas, L., Moran, S., Jost, E., & Esteller, M. (2016). DNMT3A mutations mediate the epigenetic reactivation of the leukemogenic factor MEIS1 in acute myeloid leukemia. *Oncogene*, *35*(23), 3079–3082. https://doi.org/10.1038/onc.2015.359

Fujino, T., Asada, S., Goyama, S., & Kitamura, T. (2022). Mechanisms involved in hematopoietic stem cell aging. *Cellular and Molecular Life Sciences*, *79*(9), 473. https://doi.org/10.1007/s00018-022-04356-5

Funk, J. S., Klimovich, M., Drangenstein, D., Pielhoop, O., Hunold, P., Borowek, A., Noeparast, M., Pavlakis, E., Neumann, M., Balourdas, D.-I., Kochhan, K., Merle, N., Bullwinkel, I., Wanzel, M., Elmshäuser, S., Teply-Szymanski, J., Nist, A., Procida, T., Bartkuhn, M., … Stiewe, T. (2025). Deep CRISPR mutagenesis characterizes the functional diversity of TP53 mutations. *Nature Genetics*, *57*(1), 140–153. https://doi.org/10.1038/s41588-024-02039-4

Fuster, J. J., MacLauchlan, S., Zuriaga, M. A., Polackal, M. N., Ostriker, A. C., Chakraborty, R., Wu, C.-L., Sano, S., Muralidharan, S., Rius, C., Vuong, J., Jacob, S., Muralidhar, V., Robertson, A. A. B., Cooper, M. A., Andrés, V., Hirschi, K. K., Martin, K. A., & Walsh, K. (2017). Clonal hematopoiesis associated with TET2 deficiency accelerates atherosclerosis development in mice. *Science*, *355*(6327), 842–847. https://doi.org/10.1126/science.aag1381

Fuster, J. J., & Walsh, K. (2018). Somatic Mutations and Clonal Hematopoiesis. *Circulation Research*, *122*(3), 523–532. https://doi.org/10.1161/CIRCRESAHA.117.312115

Gaudelli, N. M., Komor, A. C., Rees, H. A., Packer, M. S., Badran, A. H., Bryson, D. I., & Liu, D. R. (2017). Programmable base editing of A•T to G•C in genomic DNA without DNA cleavage. *Nature*, *551*(7681), 464–471. https://doi.org/10.1038/nature24644

Gaulin, C., Kelemen, K., & Arana Yi, C. (2022). Molecular Pathways in Clonal Hematopoiesis: From the Acquisition of Somatic Mutations to Transformation into Hematologic Neoplasm. *Life (Basel, Switzerland)*, *12*(8), 1135. https://doi.org/10.3390/life12081135

Gonzalez, A. L., Dungan, M. M., Smart, C. D., Madhur, M. S., & Doran, A. C. (2024). Inflammation Resolution in the Cardiovascular System: Arterial Hypertension, Atherosclerosis, and Ischemic Heart Disease. *Antioxidants & Redox Signaling*, *40*(4–6), 292–316. https://doi.org/10.1089/ars.2023.0284

Greaves, M., & Maley, C. C. (2012). Clonal evolution in cancer. *Nature*, *481*(7381), 306–313. https://doi.org/10.1038/nature10762

Grossmann, V., Kohlmann, A., Haferlach, C., Alpermann, T., Wild, M., Weissmann, S., Eder, C., Dicker, F., Kern, W., Schnittger, S., & Haferlach, T. (2011). Landmark Analyses of *DNMT3A* Mutations in Hematological Malignancies. *Blood*, *118*(21), 407. https://doi.org/10.1182/blood.V118.21.407.407

Gundry, M. C., Brunetti, L., Lin, A., Mayle, A. E., Kitano, A., Wagner, D., Hsu, J. I., Hoegenauer, K. A., Rooney, C. M., Goodell, M. A., & Nakada, D. (2016). Highly Efficient Genome Editing of Murine and Human Hematopoietic Progenitor Cells by CRISPR/Cas9. *Cell Reports*, *17*(5), 1453–1461. https://doi.org/10.1016/j.celrep.2016.09.092

Guo, Y. (2023). *The Roles of Heterochromatin-Associated Factors in Development and Pathogenesis* [Ph.D., The University of North Carolina at Chapel Hill]. https://www.proquest.com/docview/2816708224/abstract/B9F236214B684623PQ/1?sourcetype=Dissertations%20&%20Theses

Guryanova, O. A., Shank, K., Spitzer, B., Luciani, L., Koche, R. P., Garrett-Bakelman, F. E., Ganzel, C., Durham, B. H., Mohanty, A., Hoermann, G., Rivera, S. A., Chramiec, A. G., Pronier, E., Bastian, L., Keller, M. D., Tovbin, D., Loizou, E., Weinstein, A. R., Gonzalez, A. R., … Levine, R. L. (2016). DNMT3A mutations promote anthracycline resistance in acute myeloid leukemia via impaired nucleosome remodeling. *Nature Medicine*, *22*(12), 1488–1495. https://doi.org/10.1038/nm.4210

H, K., T, S., C, S., M, K., W, Y., A, J., Ms, N., C, G., F, P., H, B., B, P., Fb, T., & Ma, R. (2025). Continuous map of early hematopoietic stem cell differentiation across human lifetime. *Nature Communications*, *16*(1). https://doi.org/10.1038/s41467-025-57096-y

Hanson, G., & Coller, J. (2018a). Codon optimality, bias and usage in translation and mRNA decay. *Nature Reviews Molecular Cell Biology*, *19*(1), 20–30. https://doi.org/10.1038/nrm.2017.91

Hanson, G., & Coller, J. (2018b). Codon optimality, bias and usage in translation and mRNA decay. *Nature Reviews Molecular Cell Biology*, *19*(1), 20–30. https://doi.org/10.1038/nrm.2017.91

Hanson, G., & Coller, J. (2018c). Codon optimality, bias and usage in translation and mRNA decay. *Nature Reviews Molecular Cell Biology*, *19*(1), 20–30. https://doi.org/10.1038/nrm.2017.91

Hormaechea-Agulla, D., Matatall, K. A., Le, D. T., Kain, B., Long, X., Kus, P., Jaksik, R., Challen, G. A., Kimmel, M., & King, K. Y. (2021). Chronic infection drives Dnmt3a-loss-of-function clonal hematopoiesis via IFNγ signaling. *Cell Stem Cell*, *28*(8), 1428-1442.e6. https://doi.org/10.1016/j.stem.2021.03.002

Hsu, P. D., Lander, E. S., & Zhang, F. (2014). Development and Applications of CRISPR-Cas9 for Genome Engineering. *Cell*, *157*(6), 1262–1278. https://doi.org/10.1016/j.cell.2014.05.010

Huang, C., & Aghaei-Zarch, S. M. (2024). From molecular pathogenesis to therapy: Unraveling non-coding RNAs/DNMT3A axis in human cancers. *Biochemical Pharmacology*, *222*, 116107. https://doi.org/10.1016/j.bcp.2024.116107

Huang, G., Cai, X., & Li, D. (2025). Significance of targeting DNMT3A mutations in AML. *Annals of Hematology*, *104*(3), 1399–1414. https://doi.org/10.1007/s00277-024-05885-8

Hunt, R. C., Simhadri, V. L., Iandoli, M., Sauna, Z. E., & Kimchi-Sarfaty, C. (2014). Exposing synonymous mutations. *Trends in Genetics*, *30*(7), 308–321. https://doi.org/10.1016/j.tig.2014.04.006

Ito, S., D'Alessio, A. C., Taranova, O. V., Hong, K., Sowers, L. C., & Zhang, Y. (2010). Role of Tet proteins in 5mC to 5hmC conversion, ES-cell self-renewal and inner cell mass specification. *Nature*, *466*(7310), 1129–1133. https://doi.org/10.1038/nature09303

Jaiswal, S., & Ebert, B. L. (2019). Clonal hematopoiesis in human aging and disease. *Science*, *366*(6465), eaan4673. https://doi.org/10.1126/science.aan4673

Jaiswal, S., Natarajan, P., Silver, A. J., Gibson, C. J., Bick, A. G., Shvartz, E., McConkey, M., Gupta, N., Gabriel, S., Ardissino, D., Baber, U., Mehran, R., Fuster, V., Danesh, J., Frossard, P., Saleheen, D., Melander, O., Sukhova, G. K., Neuberg, D., … Ebert, B. L. (2017). Clonal Hematopoiesis and Risk of Atherosclerotic Cardiovascular Disease. *New England Journal of Medicine*, *377*(2), 111–121. https://doi.org/10.1056/NEJMoa1701719

Janakiraman, K., Sethuraman, V., & Jayaraj, G. (2025). A Review on Relevance of Nanosomes in Contemporary Therapeutics: Innovative Approach to Drug Delivery. *BioNanoScience*, *15*(1), 191. https://doi.org/10.1007/s12668-024-01778-2

Jeong, M., Park, H. J., Celik, H., Ostrander, E. L., Reyes, J. M., Guzman, A., Rodriguez, B., Lei, Y., Lee, Y., Ding, L., Guryanova, O. A., Li, W., Goodell, M. A., & Challen, G. A. (2018). Loss of Dnmt3a Immortalizes Hematopoietic Stem Cells In Vivo. *Cell Reports*, *23*(1), 1–10. https://doi.org/10.1016/j.celrep.2018.03.025

Jinek, M., Chylinski, K., Fonfara, I., Hauer, M., Doudna, J. A., & Charpentier, E. (2012). A Programmable Dual-RNA–Guided DNA Endonuclease in Adaptive Bacterial Immunity. *Science*, *337*(6096), 816–821. https://doi.org/10.1126/science.1225829

Kallikourdis, M., Cochran, J. D., Walsh, K., & Condorelli, G. (2025). Contributions of Noncardiac Organ–Heart Immune Crosstalk and Somatic Mosaicism to Heart Failure: Current Knowledge and Perspectives. *Circulation Research*, *136*(11), 1208–1232. https://doi.org/10.1161/CIRCRESAHA.125.325489

Kandarakov, O., & Belyavsky, A. (2020). Clonal Hematopoiesis, Cardiovascular Diseases and Hematopoietic Stem Cells. *International Journal of Molecular Sciences*, *21*(21), Article 21. https://doi.org/10.3390/ijms21217902

Karpova, D., Huerga Encabo, H., Donato, E., Calderazzo, S., Scherer, M., Llorian-Sopena, M., Leppä, A.-M., Würth, R., Stelmach, P., Papazoglou, D., Ferrelli, A., Ngo, S., Kotova, I., Harenkamp, S., Zimmer, K., Wolf, D., Panten, J., Reed, J., Przybylla, A., … Trumpp, A. (2025). Clonal hematopoiesis landscape in frequent blood donors. *Blood*, *145*(21), 2411–2423. https://doi.org/10.1182/blood.2024027999

Khrabrova, D. A., Yakubovskaya, M. G., & Gromova, E. S. (2021). AML-Associated Mutations in DNA Methyltransferase DNMT3A. *Biochemistry (Moscow)*, *86*(3), 307–318. https://doi.org/10.1134/S000629792103007X

Kim, S., Kim, D., Cho, S. W., Kim, J., & Kim, J.-S. (2014). Highly efficient RNA-guided genome editing in human cells via delivery of purified Cas9 ribonucleoproteins. *Genome Research*, *24*(6), 1012–1019. https://doi.org/10.1101/gr.171322.113

Kimiz-Gebologlu, I., Demirden, S. F., & Oncel, S. S. (2022). A study of the THP-1 cell line as the potential biologics production platform with the emphasis on serum-free media substitution for economic expediency. *Biotechnology Journal*, *17*(9), 2200154. https://doi.org/10.1002/biot.202200154

Klco, J. M., & Mullighan, C. G. (2021). Advances in germline predisposition to acute leukaemias and myeloid neoplasms. *Nature Reviews Cancer*, *21*(2), 122–137. https://doi.org/10.1038/s41568-020-00315-z

Kleinstiver, B. P., Pattanayak, V., Prew, M. S., Tsai, S. Q., Nguyen, N. T., Zheng, Z., & Joung, J. K. (2016). High-fidelity CRISPR–Cas9 nucleases with no detectable genome-wide off-target effects. *Nature*, *529*(7587), 490–495. https://doi.org/10.1038/nature16526

Ko, M., Huang, Y., Jankowska, A. M., Pape, U. J., Tahiliani, M., Bandukwala, H. S., An, J., Lamperti, E. D., Koh, K. P., Ganetzky, R., Liu, X. S., Aravind, L., Agarwal, S., Maciejewski, J. P., & Rao, A. (2010). Impaired hydroxylation of 5-methylcytosine in myeloid cancers with mutant TET2. *Nature*, *468*(7325), 839–843. https://doi.org/10.1038/nature09586

Komic, H., Schmachtel, T., Simoes, C., Külp, M., Yu, W., Jolly, A., Nilsson, M. S., Gonzalez, C., Prosper, F., Bonig, H., Paiva, B., Thorén, F. B., & Rieger, M. A. (2025). Continuous map of early hematopoietic stem cell differentiation across human lifetime. *Nature Communications*, *16*(1), 2287. https://doi.org/10.1038/s41467-025-57096-y

Komor, A. C., Kim, Y. B., Packer, M. S., Zuris, J. A., & Liu, D. R. (2016a). Programmable editing of a target base in genomic DNA without double-stranded DNA cleavage. *Nature*, *533*(7603), 420–424. https://doi.org/10.1038/nature17946

Komor, A. C., Kim, Y. B., Packer, M. S., Zuris, J. A., & Liu, D. R. (2016b). Programmable editing of a target base in genomic DNA without double-stranded DNA cleavage. *Nature*, *533*(7603), 420–424. https://doi.org/10.1038/nature17946

Krämer, S. J. (2023). *Uncovering the mechanisms and information content of CpG-resolved DNA methylation programming during hematopoietic differentiation* [Dissertation]. https://doi.org/10.11588/heidok.00033968

Kusne, Y., Xie, Z., & Patnaik, M. M. (2022). Clonal hematopoiesis: Molecular and clinical implications. *Leukemia Research*, *113*, 106787. https://doi.org/10.1016/j.leukres.2022.106787

Laurenti, E., & Göttgens, B. (2018). From haematopoietic stem cells to complex differentiation landscapes. *Nature*, *553*(7689), 418–426. https://doi.org/10.1038/nature25022

Lewis, C. J. T., Pan, T., & Kalsotra, A. (2017). RNA modifications and structures cooperate to guide RNA–protein interactions. *Nature Reviews Molecular Cell Biology*, *18*(3), 202–210. https://doi.org/10.1038/nrm.2016.163

Ley, T. J., Ding, L., Walter, M. J., McLellan, M. D., Lamprecht, T., Larson, D. E., Kandoth, C., Payton, J. E., Baty, J., Welch, J., Harris, C. C., Lichti, C. F., Townsend, R. R., Fulton, R. S., Dooling, D. J., Koboldt, D. C., Schmidt, H., Zhang, Q., Osborne, J. R., … Wilson, R. K. (2010). DNMT3A Mutations in Acute Myeloid Leukemia. *New England Journal of Medicine*, *363*(25), 2424–2433. https://doi.org/10.1056/NEJMoa1005143

Li, Y. (2023). Evaluating the function of DNMT3A mutations associated with Acute Myeloid Leukemia and DNMT3A Overgrowth Syndrome. *Arts & Sciences Electronic Theses and Dissertations*. https://doi.org/10.7936/trac-yq28

Liang, X., Potter, J., Kumar, S., Ravinder, N., & Chesnut, J. D. (2017). Enhanced CRISPR/Cas9-mediated precise genome editing by improved design and delivery of gRNA, Cas9 nuclease, and donor DNA. *Journal of Biotechnology*, *241*, 136–146. https://doi.org/10.1016/j.jbiotec.2016.11.011

Lin, S., Staahl, B. T., Alla, R. K., & Doudna, J. A. (2014). Enhanced homology-directed human genome engineering by controlled timing of CRISPR/Cas9 delivery. *eLife*, *3*, e04766. https://doi.org/10.7554/eLife.04766

Lino, C. A., Harper, J. C., Carney, J. P., & Timlin, J. A. (2018). Delivering CRISPR: A review of the challenges and approaches. *Drug Delivery*, *25*(1), 1234–1257. https://doi.org/10.1080/10717544.2018.1474964

Lue, N. Z.-B. (2023). *Integrating Functional Genomics and Biochemistry to Interrogate DNMT3A Sequence–Function* [Ph.D., Harvard University]. https://www.proquest.com/docview/2822173466/abstract/9BF21CC579EB4ABEPQ/1?sourcetype=Dissertations%20&%20Theses

Lyko, F. (2018). The DNA methyltransferase family: A versatile toolkit for epigenetic regulation. *Nature Reviews Genetics*, *19*(2), 81–92. https://doi.org/10.1038/nrg.2017.80

Marnell, C. S., Bick, A., & Natarajan, P. (2021). Clonal hematopoiesis of indeterminate potential (CHIP): Linking somatic mutations, hematopoiesis, chronic inflammation and cardiovascular disease. *Journal of Molecular and Cellular Cardiology*, *161*, 98–105. https://doi.org/10.1016/j.yjmcc.2021.07.004

Maruyama, T., Dougan, S. K., Truttmann, M. C., Bilate, A. M., Ingram, J. R., & Ploegh, H. L. (2015). Increasing the efficiency of precise genome editing with CRISPR-Cas9 by inhibition of nonhomologous end joining. *Nature Biotechnology*, *33*(5), 538–542. https://doi.org/10.1038/nbt.3190

Mende, N., & Laurenti, E. (2021). Hematopoietic stem and progenitor cells outside the bone marrow: Where, when, and why. *Experimental Hematology*, *104*, 9–16. https://doi.org/10.1016/j.exphem.2021.10.002

Mitra, A., Kumar, A., Amdare, N. P., & Pathak, R. (2024). Current Landscape of Cancer Immunotherapy: Harnessing the Immune Arsenal to Overcome Immune Evasion. *Biology*, *13*(5), Article 5. https://doi.org/10.3390/biology13050307

Mock, U., Hauber, I., & Fehse, B. (2016). Digital PCR to assess gene-editing frequencies (GEF-dPCR) mediated by designer nucleases. *Nature Protocols*, *11*(3), 598–615. https://doi.org/10.1038/nprot.2016.027

Morris, C., Cluet, D., & Ricci, E. P. (2021). Ribosome dynamics and mRNA turnover, a complex relationship under constant cellular scrutiny. *WIREs RNA*, *12*(6), e1658. https://doi.org/10.1002/wrna.1658

Nam, A. S., Dusaj, N., Izzo, F., Murali, R., Myers, R. M., Mouhieddine, T. H., Sotelo, J., Benbarche, S., Waarts, M., Gaiti, F., Tahri, S., Levine, R., Abdel-Wahab, O., Godley, L. A., Chaligne, R., Ghobrial, I., & Landau, D. A. (2022). Single-cell multi-omics of human clonal hematopoiesis reveals that DNMT3A R882 mutations perturb early progenitor states through selective hypomethylation. *Nature Genetics*, *54*(10), 1514–1526. https://doi.org/10.1038/s41588-022-01179-9

Natarajan, P. (2023). Genomic Aging, Clonal Hematopoiesis, and Cardiovascular Disease. *Arteriosclerosis, Thrombosis, and Vascular Biology*, *43*(1), 3–14. https://doi.org/10.1161/ATVBAHA.122.318181

Nouboussie, D. F., Whelihan, M. F., Yu, Y.-B., Sparkenbaugh, E., Pawlinski, R., Monroe, D. M., & Key, N. S. (2017). In vitro activation of coagulation by human neutrophil DNA and histone proteins but not neutrophil extracellular traps. *Blood*, *129*(8), 1021–1029. https://doi.org/10.1182/blood-2016-06-722298

Oelschlaeger, P. (2024). Molecular Mechanisms and the Significance of Synonymous Mutations. *Biomolecules*, *14*(1), Article 1. https://doi.org/10.3390/biom14010132

Ortmann, C. A., Dorsheimer, L., Abou-El-Ardat, K., Hoffrichter, J., Assmus, B., Bonig, H., Scholz, A., Pfeifer, H., Martin, H., Schmid, T., Brüne, B., Scheich, S., Steffen, B., Riemann, J., Hermann, S., Dukat, A., Bug, G., Brandts, C. H., Wagner, S., … Rieger, M. A. (2019). Functional Dominance of CHIP-Mutated Hematopoietic Stem Cells in Patients Undergoing Autologous Transplantation. *Cell Reports*, *27*(7), 2022-2028.e3. https://doi.org/10.1016/j.celrep.2019.04.064

Ozisik, G., Mantovani, G., Achermann, J. C., Persani, L., Spada, A., Weiss, J., Beck-Peccoz, P., & Jameson, J. L. (2003). An Alternate Translation Initiation Site Circumvents an Amino-Terminal DAX1 Nonsense Mutation Leading to a Mild Form of X-Linked Adrenal Hypoplasia Congenita. *The Journal of Clinical Endocrinology & Metabolism*, *88*(1), 417–423. https://doi.org/10.1210/jc.2002-021034

Pinaud, M., & Zamborlini, A. (2025). Electroporation-Based CRISPR-Cas9-Mediated Gene Knockout in THP-1 Cells and Single-Cell Clone Isolation. *Journal of Visualized Experiments (JoVE)*, *216*, e67469. https://doi.org/10.3791/67469

Porteus, M. H. (2015). Genome Editing of the Blood: Opportunities and Challenges. *Current Stem Cell Reports*, *1*(1), 23–30. https://doi.org/10.1007/s40778-014-0003-z

Reed, S. C., Croessmann, S., & Park, B. H. (2023). CHIP Happens: Clonal Hematopoiesis of Indeterminate Potential and Its Relationship to Solid Tumors. *Clinical Cancer Research*, *29*(8), 1403–1411. https://doi.org/10.1158/1078-0432.CCR-22-2598

Richardson, C. D., Ray, G. J., DeWitt, M. A., Curie, G. L., & Corn, J. E. (2016). Enhancing homology-directed genome editing by catalytically active and inactive CRISPR-Cas9 using asymmetric donor DNA. *Nature Biotechnology*, *34*(3), 339–344. https://doi.org/10.1038/nbt.3481

Roth, T. L., Puig-Saus, C., Yu, R., Shifrut, E., Carnevale, J., Li, P. J., Hiatt, J., Saco, J., Krystofinski, P., Li, H., Tobin, V., Nguyen, D. N., Lee, M. R., Putnam, A. L., Ferris, A. L., Chen, J. W., Schickel, J.-N., Pellerin, L., Carmody, D., … Marson, A. (2018). Reprogramming human T cell function and specificity with non-viral genome targeting. *Nature*, *559*(7714), 405–409. https://doi.org/10.1038/s41586-018-0326-5

Sano, S., Horitani, K., Ogawa, H., Halvardson, J., Chavkin, N. W., Wang, Y., Sano, M., Mattisson, J., Hata, A., Danielsson, M., Miura-Yura, E., Zaghlool, A., Evans, M. A., Fall, T., De Hoyos, H. N., Sundström, J., Yura, Y., Kour, A., Arai, Y., … Walsh, K. (2022). Hematopoietic loss of Y chromosome leads to cardiac fibrosis and heart failure mortality. *Science*, *377*(6603), 292–297. https://doi.org/10.1126/science.abn3100

Sano, S., Oshima, K., Wang, Y., MacLauchlan, S., Katanasaka, Y., Sano, M., Zuriaga, M. A., Yoshiyama, M., Goukassian, D., Cooper, M. A., Fuster, J. J., & Walsh, K. (2018). Tet2-Mediated Clonal Hematopoiesis Accelerates Heart Failure Through a Mechanism Involving the IL-1β/NLRP3 Inflammasome. *JACC*, *71*(8), 875–886. https://doi.org/10.1016/j.jacc.2017.12.037

Sauna, Z. E., & Kimchi-Sarfaty, C. (2011). Understanding the contribution of synonymous mutations to human disease. *Nature Reviews Genetics*, *12*(10), 683–691. https://doi.org/10.1038/nrg3051

Schaefke, B., Sun, W., Li, Y.-S., Fang, L., & Chen, W. (2018). The evolution of posttranscriptional regulation. *WIREs RNA*, *9*(5), e1485. https://doi.org/10.1002/wrna.1485

Scully, R., Panday, A., Elango, R., & Willis, N. A. (2019). DNA double-strand break repair-pathway choice in somatic mammalian cells. *Nature Reviews Molecular Cell Biology*, *20*(11), 698–714. https://doi.org/10.1038/s41580-019-0152-0

Shen, X., Song, S., Li, C., & Zhang, J. (2022). Synonymous mutations in representative yeast genes are mostly strongly non-neutral. *Nature*, *606*(7915), 725–731. https://doi.org/10.1038/s41586-022-04823-w

Shi, T., Shao, J., Ding, Y., Tang, H., Tan, X., Zhou, S., Yu, S., Wang, X., Yu, G., Feng, N., & Wang, X. (2025). Xylulose 5-phosphate fosters sustained antitumor activity of progenitor-like exhausted SLC35E2+ CD8+ T effector cells. *Cell Metabolism*, *0*(0). https://doi.org/10.1016/j.cmet.2025.06.011

Slaymaker, I. M., Gao, L., Zetsche, B., Scott, D. A., Yan, W. X., & Zhang, F. (2016). Rationally engineered Cas9 nucleases with improved specificity. *Science*, *351*(6268), 84–88. https://doi.org/10.1126/science.aad5227

Smith, Z. D., & Meissner, A. (2013). DNA methylation: Roles in mammalian development. *Nature Reviews Genetics*, *14*(3), 204–220. https://doi.org/10.1038/nrg3354

Strauss, L., Guarneri, V., Gennari, A., & Sica, A. (2021). Implications of metabolism-driven myeloid dysfunctions in cancer therapy. *Cellular & Molecular Immunology*, *18*(4), 829–841. https://doi.org/10.1038/s41423-020-00556-w

Supek, F., Miñana, B., Valcárcel, J., Gabaldón, T., & Lehner, B. (2014). Synonymous Mutations Frequently Act as Driver Mutations in Human Cancers. *Cell*, *156*(6), 1324–1335. https://doi.org/10.1016/j.cell.2014.01.051

Tajima, S., Suetake, I., Takeshita, K., Nakagawa, A., Kimura, H., & Song, J. (2022). Domain Structure of the Dnmt1, Dnmt3a, and Dnmt3b DNA Methyltransferases. In A. Jeltsch & R. Z. Jurkowska (Eds), *DNA Methyltransferases—Role and Function* (pp. 45–68). Springer International Publishing. https://doi.org/10.1007/978-3-031-11454-0_3

Tall, A. R., & Fuster, J. J. (2022). Clonal hematopoiesis in cardiovascular disease and therapeutic implications. *Nature Cardiovascular Research*, *1*(2), 116–124. https://doi.org/10.1038/s44161-021-00015-3

Todorovski, A., Wang, T.-F., Carrier, M., & Xu, Y. (2025). CHIP away at the marrow-clot connection: Inflammation, clonal hematopoiesis, and thromboembolic disease. *Blood Advances*, *9*(2), 343–353. https://doi.org/10.1182/bloodadvances.2024014430

Turpin, M., & Salbert, G. (2022). 5-methylcytosine turnover: Mechanisms and therapeutic implications in cancer. *Frontiers in Molecular Biosciences*, *9*. https://doi.org/10.3389/fmolb.2022.976862

Udroiu, I., & Sgura, A. (2021). Growing and aging of hematopoietic stem cells. *World Journal of Stem Cells*, *13*(6), 594–604. https://doi.org/10.4252/wjsc.v13.i6.594

Vijg, J., Schumacher, B., Abakir, A., Antonov, M., Bradley, C., Cagan, A., Church, G., Gladyshev, V. N., Gorbunova, V., Maslov, A. Y., Reik, W., Sharifi, S., Suh, Y., & Walsh, K. (2023). Mitigating age-related somatic mutation burden. *Trends in Molecular Medicine*, *29*(7), 530–540. https://doi.org/10.1016/j.molmed.2023.04.002

von Bonin, M., Jambor, H. K., Teipel, R., Stölzel, F., Thiede, C., Damm, F., Kroschinsky, F., Schetelig, J., Chavakis, T., & Bornhäuser, M. (2021). Clonal hematopoiesis and its emerging effects on cellular therapies. *Leukemia*, *35*(10), 2752–2758. https://doi.org/10.1038/s41375-021-01337-8

Wang, S., Hu, S., Luo, X., Bao, X., Li, J., Liu, M., Lv, Y., Zhao, C., Zeng, M., Chen, X., Unsworth, A., Jones, S., Johnson, T. W., White, S. J., Jia, H., & Yu, B. (2022). Prevalence and prognostic significance of DNMT3A- and TET2-clonal haematopoiesis-driver mutations in patients presenting with ST-segment elevation myocardial infarction. *eBioMedicine*, *78*. https://doi.org/10.1016/j.ebiom.2022.103964

Wang, X., Chen, L., Wei, J., Zheng, H., Zhou, N., Xu, X., Deng, X., Liu, T., & Zou, Y. (2025). The immune system in cardiovascular diseases: From basic mechanisms to therapeutic implications. *Signal Transduction and Targeted Therapy*, *10*(1), 166. https://doi.org/10.1038/s41392-025-02220-z

Wienert, B., Nguyen, D. N., Guenther, A., Feng, S. J., Locke, M. N., Wyman, S. K., Shin, J., Kazane, K. R., Gregory, G. L., Carter, M. A. M., Wright, F., Conklin, B. R., Marson, A., Richardson, C. D., & Corn, J. E. (2020). Timed inhibition of CDC7 increases CRISPR-Cas9 mediated templated repair. *Nature Communications*, *11*(1), 2109. https://doi.org/10.1038/s41467-020-15845-1

Xie, Z., & Zeidan, A. M. (2023). CHIPing away the progression potential of CHIP: A new reality in the making. *Blood Reviews*, *58*, 101001. https://doi.org/10.1016/j.blre.2022.101001

Yamashita, M., Dellorusso, P. V., Olson, O. C., & Passegué, E. (2020). Dysregulated haematopoietic stem cell behaviour in myeloid leukaemogenesis. *Nature Reviews Cancer*, *20*(7), 365–382. https://doi.org/10.1038/s41568-020-0260-3

Yan, X.-J., Xu, J., Gu, Z.-H., Pan, C.-M., Lu, G., Shen, Y., Shi, J.-Y., Zhu, Y.-M., Tang, L., Zhang, X.-W., Liang, W.-X., Mi, J.-Q., Song, H.-D., Li, K.-Q., Chen, Z., & Chen, S.-J. (2011). Exome sequencing identifies somatic mutations of DNA methyltransferase gene DNMT3A in acute monocytic leukemia. *Nature Genetics*, *43*(4), 309–315. https://doi.org/10.1038/ng.788

Yang, L., Guell, M., Byrne, S., Yang, J. L., De Los Angeles, A., Mali, P., Aach, J., Kim-Kiselak, C., Briggs, A. W., Rios, X., Huang, P.-Y., Daley, G., & Church, G. (2013). Optimization of scarless human stem cell genome editing. *Nucleic Acids Research*, *41*(19), 9049–9061. https://doi.org/10.1093/nar/gkt555

Yang, S., Feng, Y., Gao, W., Wang, J., Liu, Y., & Feng, J. (2025a). Genome-wide transcriptional profiling identifies *HNV1* as a hydroxyurea-responsive negative regulator of virulence in *Candida albicans*. *Cellular Signalling*, *134*, 111931. https://doi.org/10.1016/j.cellsig.2025.111931

Yang, S., Feng, Y., Gao, W., Wang, J., Liu, Y., & Feng, J. (2025b). Genome-wide transcriptional profiling identifies *HNV1* as a hydroxyurea-responsive negative regulator of virulence in *Candida albicans*. *Cellular Signalling*, *134*, 111931. https://doi.org/10.1016/j.cellsig.2025.111931

Yu, B., Roberts, M. B., Raffield, L. M., Zekavat, S. M., Nguyen, N. Q. H., Biggs, M. L., Brown, M. R., Griffin, G., Desai, P., Correa, A., Morrison, A. C., Shah, A. M., Niroula, A., Uddin, M. M., Honigberg, M. C., Ebert, B. L., Psaty, B. M., Whitsel, E. A., Manson, J. E., … National Heart, Lung, and Blood Institute TOPMed Consortium. (2021). Association of Clonal Hematopoiesis With Incident Heart Failure. *JACC*, *78*(1), 42–52. https://doi.org/10.1016/j.jacc.2021.04.085

Yu, X., Qian, N., & Wang, Y. (2023). A new risk factor associated with cardiovascular disease: Clonal hematopoiesis of indeterminate potential. *Molecular Biology Reports*, *50*(3), 2813–2822. https://doi.org/10.1007/s11033-022-08118-1

Yuan, Y., & Weidhaas, J. B. (2019). Functional microRNA binding site variants. *Molecular Oncology*, *13*(1), 4–8. https://doi.org/10.1002/1878-0261.12421

Zach, R., Annis, M., Martin-Guerrero, S. M., Alatawi, A., Chia, K. H., Meredith, M., Osborn, K., Peter, N., Pearce, W., Booth, J., Rajasekaran, M., Dias, S., Coleman-Evans, L., Foster, W. R., Harper, J. A., Herbert, A. D., Tighe, C., Reuillon, T., West, R., … Hochegger, H. (2025). *The Balance between B55α and Greatwall expression levels predicts sensitivity to Greatwall inhibition in cancer cells* (p. 2025.06.02.657035). bioRxiv. https://doi.org/10.1101/2025.06.02.657035

Zahoor, A., Khazer, R., Mehraj, I., Gani, U., Fayaz, F., Khanday, F. A., & Bhat, S. S. (2025). Aberrant DNA methylation as a key modulator of cell death pathways: Insights into cancer progression and other diseases. *Functional & Integrative Genomics*, *25*(1), 50. https://doi.org/10.1007/s10142-025-01552-x

Zha, L.-F., & Cheng, X. (2024). Clonal hematopoiesis: A shared risk factor for cardiovascular diseases and tumors. *Oncology and Translational Medicine*, *10*(1), 35. https://doi.org/10.1097/ot9.0000000000000029

Zhang, M., Wang, J., Qi, G., Xie, L., Tian, Q., Yang, H., Feng, L., Zhu, N., Pan, X., Zhu, J., Hu, J., Chen, P., & Lu, H. (2025). *DNMT3A Deficiency Reduces DNMT3B Gene Methylation and Contributes to Whole-genome Transcription Alterations in HEK293 Cells*. https://doi.org/10.2174/0113892029351729250217113313

Zhang, Q., & Wang, Y. (2008). High mobility group proteins and their post-translational modifications. *Biochimica et Biophysica Acta (BBA) - Proteins and Proteomics*, *1784*(9), 1159–1166. https://doi.org/10.1016/j.bbapap.2008.04.028

Zhang, Y. (2023a). *Exploring the Interplay Between MRNA Degradation and Ribosome Dynamics Using High-Throughput Sequencing* [Ph.D., Karolinska Institutet (Sweden)]. https://www.proquest.com/docview/3073249547/abstract/D8A38F1A23D74129PQ/1?sourcetype=Dissertations%20&%20Theses

Zhang, Y. (2023b). *Exploring the Interplay Between MRNA Degradation and Ribosome Dynamics Using High-Throughput Sequencing* [Ph.D., Karolinska Institutet (Sweden)]. https://www.proquest.com/docview/3073249547/abstract/63824988F23C42C1PQ/1?sourcetype=Dissertations%20&%20Theses

Zhao, H. G., & Deininger, M. (2023). Always stressed but never exhausted: How stem cells in myeloid neoplasms avoid extinction in inflammatory conditions. *Blood*, *141*(23), 2797–2812. https://doi.org/10.1182/blood.2022017152